Article

Nociceptive nerves regulate haematopoietic stem cell mobilization

https://doi.org/10.1038/s41586-020-03057-y

Received: 4 November 2019

Accepted: 19 November 2020

Published online: 23 December 2020

Check for updates

Xin Gao[1,2], Dachuan Zhang[1,2,5], Chunliang Xu[1,2,5], Huihui Li[1,2], Kathleen M. Caron[3] & Paul S. Frenette[1,2,4]✉

Haematopoietic stem cells (HSCs) reside in specialized microenvironments in the bone marrow—often referred to as 'niches'—that represent complex regulatory milieux influenced by multiple cellular constituents, including nerves[1,2]. Although sympathetic nerves are known to regulate the HSC niche[3–6], the contribution of nociceptive neurons in the bone marrow remains unclear. Here we show that nociceptive nerves are required for enforced HSC mobilization and that they collaborate with sympathetic nerves to maintain HSCs in the bone marrow. Nociceptor neurons drive granulocyte colony-stimulating factor (G-CSF)-induced HSC mobilization via the secretion of calcitonin gene-related peptide (CGRP). Unlike sympathetic nerves, which regulate HSCs indirectly via the niche[3,4,6], CGRP acts directly on HSCs via receptor activity modifying protein 1 (RAMP1) and the calcitonin receptor-like receptor (CALCRL) to promote egress by activating the $G\alpha_s$/adenylyl cyclase/cAMP pathway. The ingestion of food containing capsaicin—a natural component of chili peppers that can trigger the activation of nociceptive neurons—significantly enhanced HSC mobilization in mice. Targeting the nociceptive nervous system could therefore represent a strategy to improve the yield of HSCs for stem cell-based therapeutic agents.

The ability to migrate is a hallmark of HSCs, which travel to different haematopoietic sites during development and continue to be released from the adult bone marrow throughout life. The migratory property of HSCs has facilitated their collection from blood and their transplantation for curative anticancer therapies. The detailed mechanisms by which HSCs migrate out of the bone marrow, however, remain largely unknown. Additionally, in some donors the yield of mobilized HSCs can be insufficient[7], indicating the need for improved methods to stimulate their mobilization.

In tissues that are exposed to the external environment—for example skin, lung and gut—nociceptor sensory neurons detect damaging stimuli, and can regulate the ensuing immune response by releasing neurotransmitters and other regulatory molecules[8–10]. However, other than the perception of pain, the role of nociceptors in a deep tissue such as the bone marrow is not well understood.

Neural collaboration to maintain HSCs

We surveyed the total nerve densities in the bone marrow by analysing expression of the pan-neuronal marker class III β tubulin (TUBB3) using immunofluorescence. Although adrenergic fibres from the sympathetic nervous system—identified by anti-tyrosine hydroxylase (TH)—comprised a meaningful fraction of the nerve staining area, the vast majority of the staining area (around 77%) consisted of nociceptive nerves marked by CGRP (Fig. 1a, b, Extended Data Fig. 1a). Analysis of total nerve length per area of bone marrow revealed that $CGRP^+$ and TH^+ nerves had similar length densities (Extended Data Fig. 1b); this suggests that both $CGRP^+$ and TH^+ nerves exhibit similar projections in the bone marrow, and that the increased area occupied by nociceptive nerves could reflect their larger bundles.

Given their afferent functions, it is possible that nociceptor neurons sense the bone marrow environment and relay these signals to the central nervous system to circuit back via efferent fibres from the sympathetic nervous system. Alternatively, nociceptors might exert efferent influences and directly alter organ physiology[9]. To distinguish between these possibilities, we treated wild-type C57BL/6 mice systemically with either vehicle, resiniferatoxin (RTX), 6-hydroxydopamine (6OHDA) or both to differentially ablate nociceptive (RTX) or sympathetic (6OHDA) nerve fibres (Extended Data Fig. 1c–e). Although sympathetic denervation significantly suppressed B lymphopoiesis—in line with previous studies[11]—neither sympathetic nor sensory denervation alone altered the number of HSCs in the bone marrow (Extended Data Fig. 2a–d). However, the dual denervation induced significant HSC expansion and led to a myeloid bias of haematopoiesis (Extended Data Fig. 2a–d). Competitive transplantation experiments revealed a marked reduction in long-term reconstitution after dual denervation compared with the other groups (Extended Data Fig. 2e, f). However, the homing efficiency of HSCs and $Lin^-Sca\text{-}1^+Kit^+$ (LSK) cells was similar between the control and dual denervation groups, suggesting that the reduced bone marrow reconstitution is independent of HSC homing (Extended Data Fig. 2g, h).

[1]Ruth L. and David S. Gottesman Institute for Stem Cell and Regenerative Medicine Research, Albert Einstein College of Medicine, New York, NY, USA. [2]Department of Cell Biology, Albert Einstein College of Medicine, New York, NY, USA. [3]Department of Cell Biology and Physiology, University of North Carolina at Chapel Hill, Chapel Hill, NC, USA. [4]Department of Medicine, Albert Einstein College of Medicine, New York, NY, USA. [5]These authors contributed equally: Dachuan Zhang, Chunliang Xu. ✉e-mail: paul.frenette@einsteinmed.org

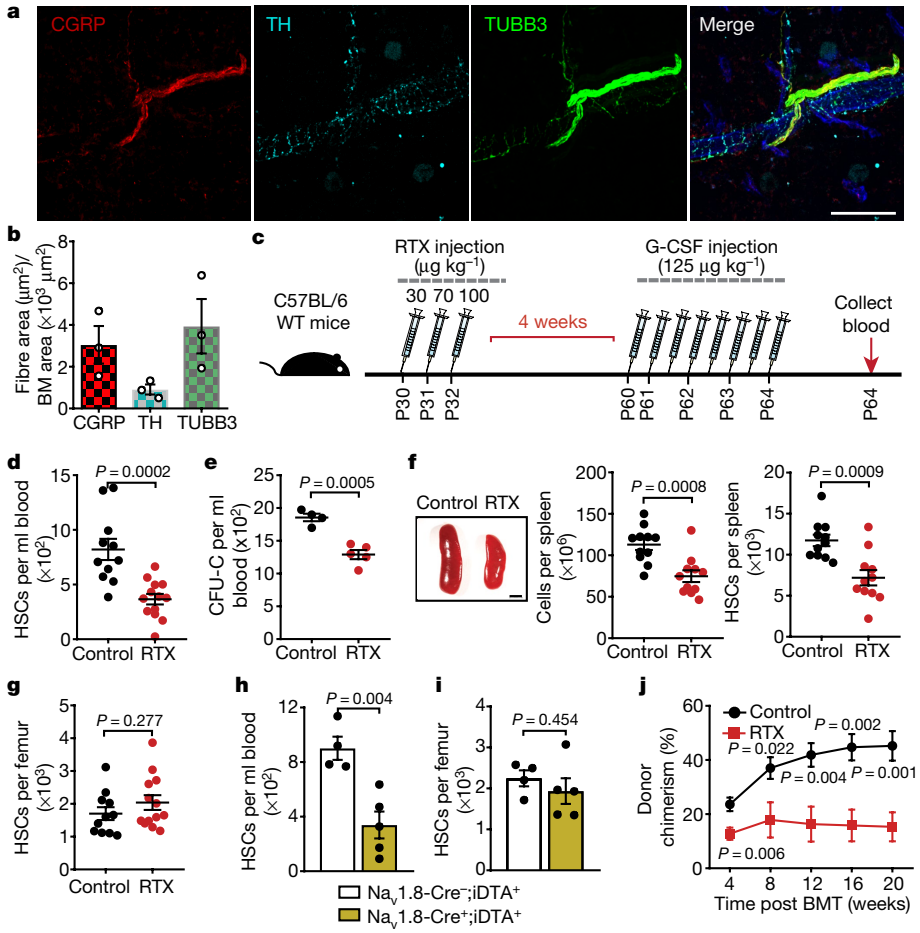

Fig. 1 | Nociceptive neurons promote HSC mobilization. a, Representative confocal *z*-stack projection of C57BL/6 mouse femur stained for CGRP (red), TH (light blue) and TUBB3 (green) nerve fibres. Scale bar, 100 µm. **b**, Femoral sensory and sympathetic innervation quantified by $CGRP^+$, TH^+ or $TUBB3^+$ stained area divided by total bone marrow (BM) area. $n = 3$ mice. **c**, Schematic of G-CSF-induced HSC mobilization experiments and analyses. P, postnatal day. **d**, Absolute numbers of HSCs ($Lin^-Sca\text{-}1^+Kit^+CD150^+CD48^-$) per ml of peripheral blood after G-CSF-induced mobilization in saline-treated (control) or RTX-treated mice. $n = 11, 13$ mice, respectively. **e**, Colony-forming units (burst-forming unit-erythroid (BFU-E), colony-forming unit-granulocyte, macrophage (CFU-GM), and colony-forming unit-granulocyte, erythroid, macrophage, megakaryocyte (CFU-GEMM)) per ml of G-CSF-mobilized blood from saline-treated or RTX-treated mice. $n = 4, 5$ mice, respectively. **f**, Left, representative images of the spleen after G-CSF-induced mobilization in saline-treated or RTX-treated mice. Scale bar, 2 mm. Middle and right, cellularity (middle) and absolute numbers of HSCs (right) in the spleens of saline-treated and RTX-treated mice after the administration of G-CSF. $n = 11$ mice per group. **g**, The number of HSCs per femur from saline-treated or RTX-treated mice after the administration of G-CSF. $n = 11, 13$ mice, respectively. **h**, **i**, The number of HSCs per ml of peripheral blood (**h**) or bone marrow HSCs per femur (**i**) after G-CSF mobilization in $Na_v1.8\text{-}Cre^-;iDTA^+$ and $Na_v1.8\text{-}Cre^+;iDTA^+$ mice. $n = 4, 5$ mice, respectively. **j**, Peripheral blood donor chimerism ($CD45.2^+$) in CD45.1-recipient mice transplanted with mobilized blood (CD45.2) derived from saline-treated or RTX-treated mice mixed with CD45.1 competitor bone marrow cells at the indicated time points after bone marrow transplantation (BMT). $n = 9, 8$ mice, respectively. Data are mean ± s.e.m. Significance was assessed using a two-tailed unpaired Student's *t*-test.

To further investigate the dual denervation in a genetic model, we intercrossed $Na_v1.8$-Cre transgenic mice with Cre-inducible diphtheria toxin A (iDTA) mice in order to specifically ablate $Na_v1.8$-expressing sensory neurons (Extended Data Fig. 3a–d). Analysis of bone marrow from $Na_v1.8$-Cre;iTdTomato mice using confocal immunofluorescence microscopy revealed that all $CGRP^+$ nerves were $iTdTomato^+$ and that the majority (more than 70%) of $Na_v1.8^+$ nociceptive nerves were $CGRP^+$ (Extended Data Fig. 3a). Dual depletion using $Na_v1.8$-Cre;iDTA mice combined with 6OHDA treatment completely recapitulated the haematopoietic phenotype that was observed after dual treatment with RTX and 6OHDA (Extended Data Fig. 3e, f). These results show that nociceptive and sympathetic nerves do not act as a circuit, but instead collaborate as parallel efferent regulators to maintain HSCs in bone marrow niches.

Nociceptor neurons secrete two major neurotransmitters, CGRP and substance P[10]. We therefore evaluated the specific contributions of these neurotransmitters, together with adrenergic signals, to the regulation of HSCs. We found that the continuous delivery of CGRP—but not substance P—returned the numbers of HSCs, B cells and myeloid cells to control levels (Extended Data Fig. 3g). HSC numbers were also restored to control levels by the administration of a pan-β-adrenergic receptor agonist (Extended Data Fig. 3g), which further indicates that nociceptive and sympathetic nerves form an integrated efferent innervation network that regulates steady-state HSC function.

Nociceptors regulate HSC mobilization

The mobilization of HSCs by G-CSF is controlled in part by peripheral sympathetic nerve-derived noradrenaline signalling via regulation of the bone marrow niche[3]. We explored the possibility that nociceptor nerve-derived neurotransmitter release in the bone marrow microenvironment might also influence G-CSF-induced HSC mobilization. Notably, the RTX-induced ablation of nociceptor neurons alone led to a marked reduction of mobilized phenotypic HSCs and colony-forming

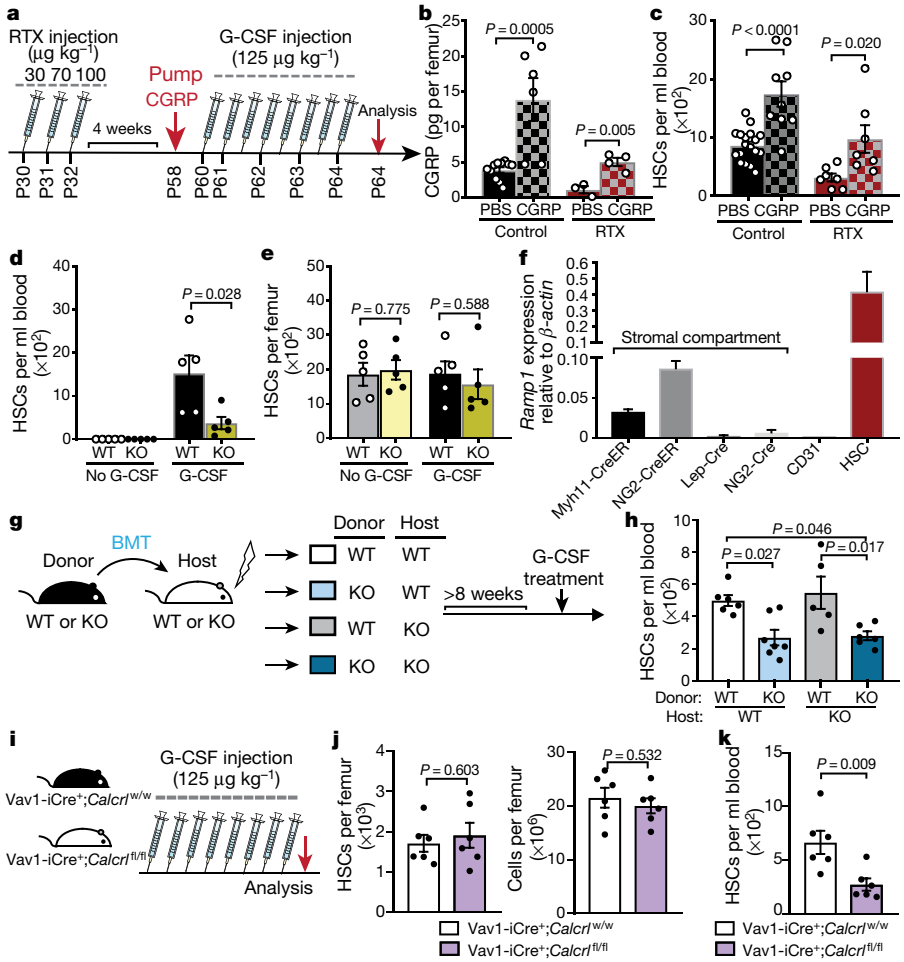

Fig. 2 | Nociceptor-derived CGRP induces HSC mobilization via its cognate receptor CALCRL–RAMP1. a, Schematic of the rescue experiment. **b**, CGRP levels in the bone marrow extracellular fluid (BMEF) measured by ELISA ($n = 11, 6, 3, 4$ mice, respectively). **c**, Absolute numbers of HSCs ($Lin^-Sca\text{-}1^+Kit^+CD150^+CD48^-$) per ml of peripheral blood after G-CSF mobilization in saline-treated or RTX-treated mice implanted with osmotic pumps containing saline or CGRP. $n = 18, 9, 7, 7$ mice, respectively. **d**, **e**, The number of HSCs per ml of peripheral blood (**d**) and per femur (**e**) from *Ramp1*$^{+/+}$ (WT) or *Ramp1*$^{-/-}$ (KO) mice with or without the administration of G-CSF. $n = 5$ mice per group. **f**, *Ramp1* mRNA levels in sorted HSCs, endothelial (CD31) and stromal compartments (from RNA sequencing datasets[5,28]). **g**, Schematic of the reciprocal transplantation of bone marrow cells from *Ramp1*$^{-/-}$ (KO) or *Ramp1*$^{+/+}$ (WT) mice into lethally irradiated *Ramp1*$^{+/+}$ (WT) or *Ramp1*$^{-/-}$ (KO) recipients. G-CSF was injected 8 weeks after transplantation. **h**, HSCs per ml of peripheral blood following G-CSF treatment after reciprocal transplantation. $n = 6, 7, 5, 6$ mice, respectively. **i**, Schematic of mobilization experiment with Vav1-iCre$^+$;*Calcrl*$^{fl/fl}$ mice. **j**, **k**, Absolute numbers of HSCs (**j**, left) and cellularity (**j**, right) in femurs, and number of HSCs per ml of blood (**k**) after G-CSF treatment in Vav1-iCre$^+$;*Calcrl*$^{w/w}$ or Vav1-iCre$^+$;*Calcrl*$^{fl/fl}$ mice. $n = 6$ mice per group. Data are mean ± s.e.m. Significance was assessed using a two-tailed unpaired Student's *t*-test (**b**–**e**, **j**, **k**) or one-way ANOVA (**h**).

progenitors (Fig. 1c–e) and LSK cells (Extended Data Fig. 4a) in response to G-CSF when compared to vehicle-treated control mice. Consistent with the reduced mobilization, the size of the spleen and its HSC content were significantly reduced in RTX-treated mice compared to nerve-intact mice (Fig. 1f, Extended Data Fig. 4b). However, we observed no haematopoietic deficits in the bone marrow (Fig. 1g, Extended Data Fig. 4c, d), which suggests that the absence of nociceptor neurons selectively affected HSC egress. We obtained similar results using $Na_v1.8$-Cre;iDTA mice (Fig. 1h, i, Extended Data Fig. 4e, f). To assess the blood content in functional HSCs, we transfused blood from G-CSF-, vehicle- or RTX-treated mice mixed with competitor bone marrow cells into lethally irradiated recipients. Mice reconstituted with the mobilized blood from the RTX-treated mice consistently exhibited lower donor multi-lineage reconstitution 20 weeks after transplantation (Fig. 1j, Extended Data Fig. 4g, h). These data indicate that nociceptor neurons are required to drive robust G-CSF-elicited HSC mobilization from the bone marrow into the blood.

The neuropeptide CGRP promotes HSC egress

Because CGRP was found to collaborate with adrenergic signals in HSC maintenance, we next investigated its role in HSC mobilization (Fig. 2a). Treatment with CGRP resulted in significantly increased CGRP levels in the bone marrow extracellular fluid (Fig. 2b) and substantially increased the number of HSCs mobilized by G-CSF (Fig. 2c). By contrast, no statistically significant improvement in HSC mobilization was observed after the administration of substance P (Extended Data Fig. 5a, b). Moreover, CGRP administration rescued the mobilization deficit of mice that lacked nociceptors to levels similar to those observed in saline-treated wild-type control mice (Fig. 2c). Although the administration of CGRP did not alter the cellularity of the bone marrow, it significantly reduced the number of bone marrow HSCs (Extended Data Fig. 5c), consistent with previous studies suggesting that sustained CGRP treatment might suppress the proliferation of haematopoietic stem and progenitor cells (HSPCs)[12]. To further exclude the possibility that nociceptive neurons could act via a sympathetic efferent circuit, we depleted sympathetic nerves using 6OHDA and evaluated whether CGRP could still induce HSC mobilization. We found that CGRP treatment led to a significant and proportional (around threefold) increase in HSC mobilization in the absence of sympathetic neurons (Extended Data Fig. 5d). These results suggest that G-CSF-induced HSC mobilization is regulated by the nociceptor nerve-derived neuropeptide CGRP.

To investigate how CGRP promotes HSC egress, we evaluated the function of the CGRP receptor, which is formed by heterodimers of CALCRL and RAMP1, both of which are required to initiate a response to CGRP. We examined G-CSF-induced HSC mobilization in *Ramp1*$^{-/-}$ mice compared with *Ramp1*$^{+/+}$ littermates (Extended Data Fig. 6a), and found a marked reduction in G-CSF-induced HSC mobilization in mice that lacked *Ramp1* (Fig. 2d). The reduction of mobilized HSCs in *Ramp1*$^{-/-}$ mice was not due to lower HSC reserves in the bone marrow (Fig. 2e). Additionally, we found no haematopoietic deficit at steady state, and *Ramp1* deficiency did not affect the homing ability of HSCs and LSK cells to the bone marrow (Extended Data Fig. 6b–f). These findings indicate that *Ramp1* deletion selectively impairs HSC egress into the circulation.

CGRP acts on haematopoietic cells

To identify which cells are the target of nociceptors, we first measured *Ramp1* expression levels in various stromal and haematopoietic

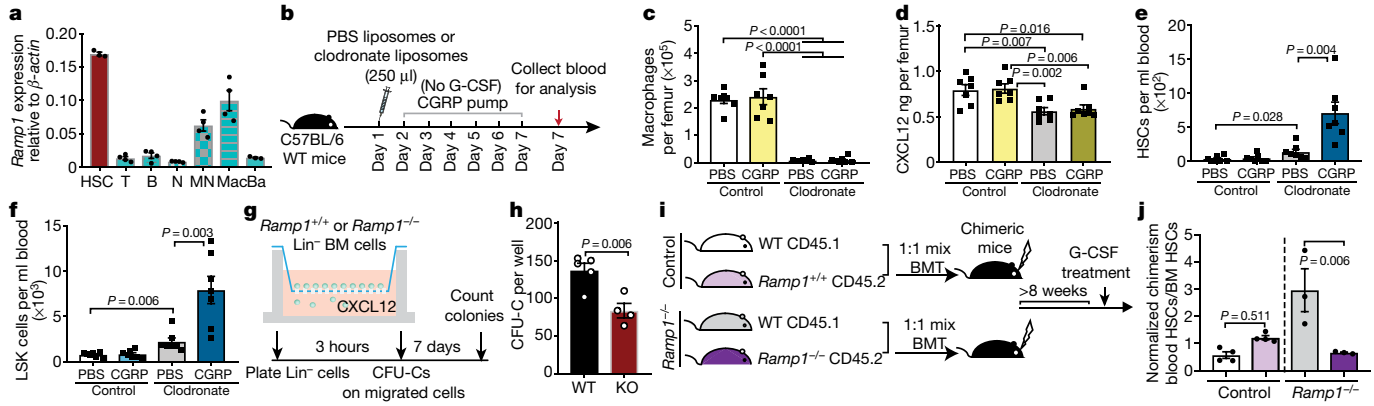

Fig. 3 | RAMP1 signals directly in HSCs. a. Quantification by RT–PCR of *Ramp1* mRNA levels in sorted T lymphocytes (T), B lymphocytes (B), neutrophils (N), monocytes (MN), macrophages (Mac) and basophils (Ba) from the bone marrow. $n = 3$–4 biologically independent samples. **b**, Schematic of the macrophage depletion experiment. **c**, Number of macrophages ($Gr\text{-}1^-F4/80^+CD115^{int}SSC^{int/low}$) per femur from PBS-treated (control) or clodronate-liposome-treated mice implanted with osmotic pumps containing saline or CGRP. $n = 7$ mice per group. **d**, CXCL12 levels in bone marrow extracellular fluid measured by ELISA. $n = 7$ biological samples. **e**, **f**, HSCs ($Lin^-Sca\text{-}1^+cKit^+CD150^+CD48^-$) (**e**) and LSK cells ($Lin^-Sca\text{-}1^+Kit^+$) (**f**) per ml of peripheral blood. $n = 7$ mice per group. **g**, Experimental design of the transwell assay. **h**, Colony-forming units per well of migrated stem progenitor cells from $Ramp1^{+/+}$ (WT) or $Ramp1^{-/-}$ (KO) mice. $n = 5, 4$ mice, respectively. **i**, Schematic of the mixed chimerism experiment. **j**, Chimerism of mobilized HSCs in blood normalized to the chimerism of bone marrow HSCs. $n = 4, 4, 3, 3$ mice, respectively. Data are mean ± s.e.m. Significance was assessed using a two-tailed unpaired Student's *t*-test (**c**–**f**, **h**) or one-way ANOVA (**j**).

elements. Whereas *Ramp1* was expressed at low levels in stromal cells, robust expression was detected in HSCs (Fig. 2f). To ascertain whether *Ramp1* was required in the haematopoietic or the stromal compartment of the bone marrow, we generated chimeric mice by reciprocal transplantation of bone marrow cells from $Ramp1^{-/-}$ or $Ramp1^{+/+}$ mice into lethally irradiated $Ramp1^{+/+}$ or $Ramp1^{-/-}$ recipients (Fig. 2g). We found that the mobilization defect in the $Ramp1^{-/-}$ recipients was rescued when donor HSCs were wild type (Fig. 2h). By contrast, chimaeras in which $Ramp1^{-/-}$ donor HSCs engrafted wild-type recipients exhibited the same reduction in HSC mobilization (Fig. 2h) without alteration of cellularity or HSC numbers in the bone marrow (Extended Data Fig. 6g). To confirm the haematopoietic origin of the defect, we intercrossed $Calcrl^{fl/fl}$ mice with Vav1-iCre mice to conditionally delete *Calcrl* in haematopoietic cells (Fig. 2i). We found a similar HSC mobilization defect in Vav1-iCre$^+$;$Calcrl^{fl/fl}$ mice, whereas the number of HSCs and the cellularity of the bone marrow were not altered (Fig. 2j, k). In addition, we did not observe any significant changes in the number of niche-associated cells or in CXCL12 expression within distinct niche compartments (Extended Data Fig. 7a–c). We therefore conclude that CGRP acts on haematopoietic cells, via its heterodimeric receptor RAMP1–CALCRL, to promote HSC egress.

Next we sought to define the haematopoietic cell type that is targeted by CGRP and that regulates HSC mobilization. Analysis by quantitative (real-time) PCR (qPCR) revealed that the expression of *Ramp1* was highest in HSCs, with lower expression in monocytes and macrophages (Fig. 3a). We therefore investigated the role of monocytes and macrophages, both of which are known to regulate HSC mobilization[13–15]. Depletion of bone marrow monocytes and macrophages using clodronate liposome[13–15] significantly reduced levels of CXCL12 in the bone marrow, leading to a significant increase of HSPCs in the blood (Fig. 3b–f). Notably, the administration of CGRP to mice depleted of mononuclear cells markedly enhanced HSC mobilization without affecting CXCL12 levels in the bone marrow (Fig. 3e, f). The synergistic effect of CGRP administration and mononuclear cell depletion excludes the possibility that CGRP is acting on mononuclear phagocytes to promote HSC mobilization.

To address whether CGRP/RAMP1 signals were HSPC autonomous, we analysed the migration capacity of haematopoietic progenitors towards the chemoattractant CXCL12 (Fig. 3g). These analyses revealed that the transmigration of lineage-depleted progenitor cells from $Ramp1^{-/-}$ mice was significantly reduced (Fig. 3h). To confirm the HSPC autonomous effect in vivo, we generated mixed chimaeras in which $CD45.1^+$ recipient mice were transplanted with a mix of bone marrow from $CD45.1^+$ wild-type and $CD45.2^+$ $Ramp1^{-/-}$ or $Ramp1^{+/+}$ mice at a 1:1 ratio (Fig. 3i). These analyses revealed significant impairments in the mobilization of $Ramp1^{-/-}$ HSCs from the bone marrow (Fig. 3j), further suggesting that CGRP acts directly on HSPCs.

CGRP activates $G\alpha_s$–adenylyl cyclase–cAMP pathways

We found no change in the expression of receptors involved in HSC trafficking (CXCR4, VLA4 or CD44) after the administration of CGRP, which suggests a mechanism that is independent of these receptors (Extended Data Fig. 7d). To obtain further mechanistic insight, we analysed genome-wide changes in gene expression in purified HSCs from $Ramp^{+/+}$ and $Ramp1^{-/-}$ mice by RNA sequencing (Fig. 4a, Extended Data Fig. 8a). Gene set enrichment analysis revealed the downregulation of genes associated with $G\alpha_s$–adenylyl cyclase–cAMP pathways, including cAMP-dependent protein kinase A-mediated phosphorylation of cAMP-response element binding (CREB) and activation of extracellular-signal-regulated kinases (ERKs) (Extended Data Fig. 8b, c). Because $G\alpha_s$ can activate adenylyl cyclase to generate cAMP, we tested whether stimulation of adenylyl cyclase with forskolin could rescue the mobilization defect of *Ramp1*-deficient HSCs. We found that activation of adenylyl cyclase completely restored G-CSF-mobilized HSCs in $Ramp1^{-/-}$ mice (Fig. 4b), without affecting the number of bone marrow HSCs (Fig. 4c). These results indicate that the CGRP–RAMP1 pathway promotes HSC mobilization via the activation of downstream $G\alpha_s$–adenylyl cyclase–cAMP signalling.

The CGRP-induced activation of the $G\alpha_s$–adenylyl cyclase–cAMP pathway in HSCs suggested the possibility of an additive effect with plerixafor (AMD3100), an antagonist of CXCR4 that is approved by the US Food and Drug Administration (FDA) and is administered alongside G-CSF to elicit HSPCs in patients who show a poor mobilization response or in patients for whom G-CSF is contraindicated[7,16]. The administration of plerixafor with CGRP markedly increased HSC mobilization compared with the administration of plerixafor alone (Fig. 4d). Notably, CGRP administration further increased the mobilization induced by concurrent treatment with plerixafor and G-CSF (Fig. 4e), and this was confirmed by long-term competitive repopulation of mobilized blood (Fig. 4f). To investigate whether adrenergic stimulation could enhance HSC mobilization induced by CGRP,

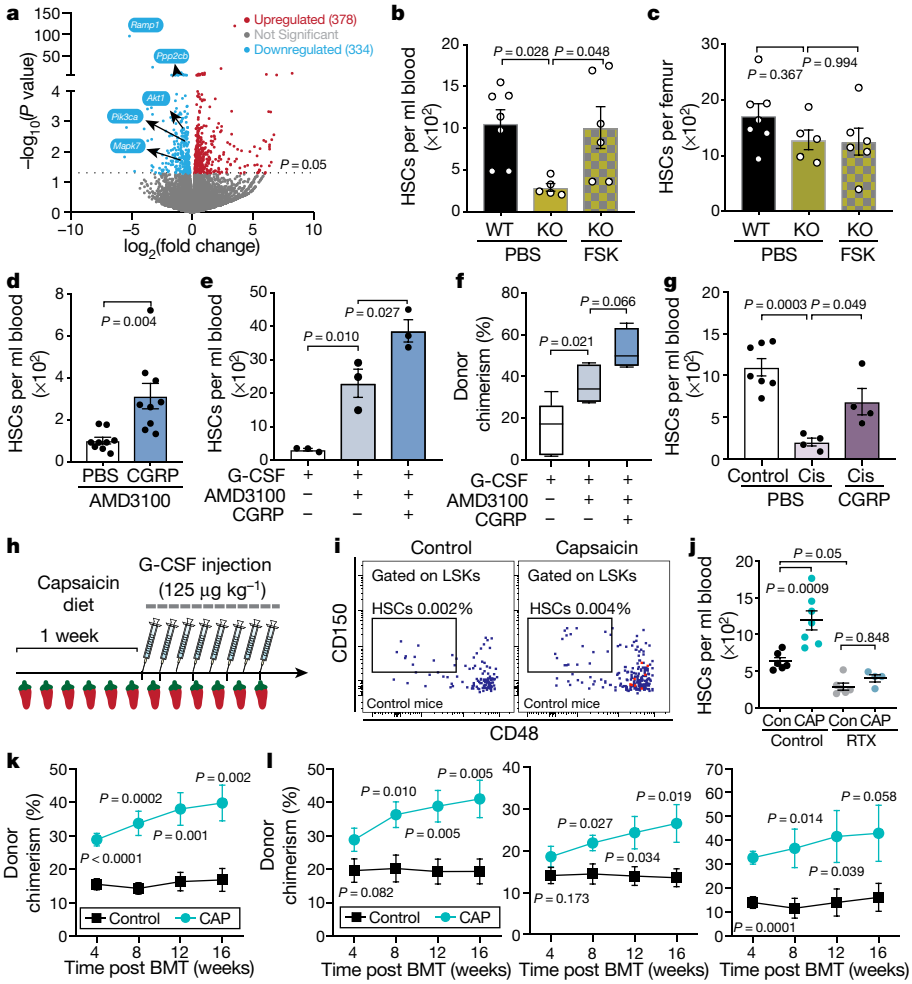

Fig. 4 | CGRP amplifies HSC mobilization via the $G\alpha_s$–adenylyl cyclase–cAMP pathway. a, Volcano plot showing differentially expressed genes ($P < 0.05$) in *Ramp1*$^{-/-}$ compared to *Ramp1*$^{+/+}$ HSCs. **b**, **c**, Absolute numbers of HSCs per ml of blood (**b**) or per femur (**c**) after G-CSF administration in *Ramp1*$^{+/+}$ and *Ramp1*$^{-/-}$ mice treated with vehicle (PBS) or forskolin (FSK). $n = 7, 5, 6$ mice, respectively. **d**, The number of HSCs in plerixafor-mobilized blood from saline-treated or CGRP-treated mice. $n = 9$ mice per group. **e**, HSCs per ml of blood from mice treated with G-CSF, G-CSF + AMD3100 or G-CSF + AMD3100 + CGRP. $n = 3$ mice per group. **f**, Blood donor chimerism (CD45.2) in CD45.1-recipient mice transplanted with mobilized blood (CD45.2) mixed with CD45.1 competitor bone marrow cells, 16 weeks after transplantation. $n = 5$ mice per group. **g**, The number of HSCs in G-CSF-mobilized blood of saline-treated or cisplatin (cis)-treated mice with or without the administration of CGRP. $n = 7, 4, 4$ mice, respectively. **h**, Experimental design to determine the effect of a capsaicin-containing diet on HSC mobilization. **i**, **j**, Representative gating strategy (**i**) and quantification (**j**) of HSCs per ml of blood after G-CSF administration in saline-treated or RTX-treated mice fed on a control diet or a capsaicin (CAP)-containing diet. $n = 6, 7, 6, 4$ mice, respectively. **k**, **l**, Blood leukocyte chimerism in total blood (**k**) and blood B cells (**l**, left), T cells (**l**, middle) and myeloid cells (**l**, right) of CD45.1-recipient mice transplanted with mobilized blood (CD45.2) derived from mice fed on control or capsaicin diets mixed with CD45.1 competitor bone marrow cells. $n = 9$ mice per group. Data are mean ± s.e.m. Significance was assessed using a two-tailed unpaired Student's *t*-test (**d**, **k**, **l**) or one-way ANOVA (**b**, **c**, **e**–**g**, **j**). For box plots, the box spans from the 25th to 75th percentiles and the centre line shows the median. Whiskers represent minimum to maximum range.

we treated mice with the noradrenaline reuptake inhibitor desipramine, which enhances HSC mobilization by increasing the adrenergic tone in the bone marrow[17,18]. However, we did not observe further mobilization when combining desipramine and CGRP stimulation (Extended Data Fig. 8d, e), which suggests that they might be acting on the same mobilizable pool. To assess whether CGRP administration could rescue the defective HSC mobilization from diseased bone marrow, we evaluated mice that had received multiple cycles of chemotherapy—a common cause of insufficient HSC yield in the clinic[19]. As expected[4], G-CSF-induced HSPC mobilization was significantly impaired in mice treated with cisplatin, and we found that this deficit was significantly rescued by CGRP administration (Fig. 4g). These data suggest that CGRP-induced signals broadly contribute to HSC egress.

Spicy food enhances HSC mobilization

The role of nociceptors in promoting HSC mobilization led us to hypothesize that the ingestion of spicy food—which can trigger nociceptive nerve activation—could influence HSC mobilization from the bone marrow. To explore this possibility, we fed C57BL/6 mice a diet containing capsaicin—a chili pepper extract and natural ligand that activates TRPV1$^+$ neurons (Fig. 4h, Extended Data Fig. 9a). When given the choice, mice preferred regular chow over spicy chow; however, their daily food intake and body weight were not altered on a spicy food diet (Extended Data Fig. 9b, c). Mice given a capsaicin-containing diet had significantly increased CGRP levels in the bone marrow extracellular fluid, with no change in the number of HSCs or in their proliferation (Extended Data Fig. 9d, e). Notably, G-CSF-induced HSPC egress in mice that consumed spicy food was significantly higher than in those fed with standard chow (Fig. 4i, j, Extended Data Fig. 9f). This was confirmed by competitive repopulation assays of mobilized blood (Fig. 4k, l). By contrast, capsaicin did not enhance HSC mobilization when nociceptors were depleted by treatment with RTX (Fig. 4j); this indicates that capsaicin probably acts via nociceptors, although additional mechanisms remain possible. To determine whether the increased repopulation activity seen in mice that were fed a capsaicin diet was due to the increased

numbers or an increased engraftment capacity of HSCs, we carried out competitive repopulation experiments with sorted HSCs. We found no difference in the repopulation activities between the capsaicin-treated and control groups (Extended Data Fig. 9g–j). Similar results were obtained with sorted HSCs from mice stimulated with CGRP (Extended Data Fig. 9k–m). These results suggest that the increased bone marrow repopulation activity elicited by the capsaicin diet or by CGRP administration did not result from enhanced HSC competitiveness, but from a greater number of mobilized functional HSCs.

Discussion

Nociceptors enable the rapid detection of external insults—such as pain, cold or heat—to avoid organ damage[8,10]. Although nociceptors are integral to the generation of an immune response to protect the integrity of the body, our results uncover a role for nociceptor neurons in an organ that is isolated from the external environment, in which nerve-derived CGRP release regulates HSC maintenance and egress from the bone marrow (Extended Data Fig. 10). CGRP acts via CALCRL–RAMP1 receptors expressed on HSPCs, which leads to an increase in the level of $G\alpha_s$-mediated cAMP that promotes the egress of HSPCs. These results are in line with previous studies suggesting that $G\alpha_s$ enhances HSC mobilization via a then-unidentified GPCR[20]. It is notable that the interaction of prostaglandin E_2 with the $G\alpha_s$-coupled E-prostanoid receptor-4 (EP4) also induces an increase in cAMP, which regulates HSPC homing and mobilization[21,22]. Prostaglandin E_2 enhances homing in part by increasing CXCR4 expression on HSPCs, whereas the inhibition of EP4 signalling in stromal cells (not HSPCs) promotes HSPC egress[21,22]. By contrast, CGRP alters neither CXCR4 expression nor homing to bone marrow. The differing responses to increased levels of cAMP by different GPCRs could involve different CREB-dependent or -independent mechanisms[23] and/or the activation of co-signalling pathways that might specify the response.

The administration of G-CSF is frequently associated with bone pain, which is often reported after the first dose[24]; this is consistent with the present results suggesting that pain probably arises from the activation of nociceptive neurons rather than from a rapid increase in the number of haematopoietic cells in the confined bone marrow space. Consistent with this, G-CSF has been reported to activate directly receptors expressed on sensory neurons, release CGRP and cause pain[25]. Three antibody drugs that target CGRP have recently been approved by the FDA and the European Medicines Agency to treat migraine[26]. On the basis of the present results, the inhibition of CGRP would interfere with HSC mobilization. Conversely, TRPV1 receptor agonists have been formulated for pain relief[27] and, if administered at relatively low doses, could act as a substitute for the ingestion of the 10 jalapeño peppers a day for 4 days that is predicted to enhance HSC mobilization in humans. Enhancing signals from the nociceptive nervous system could therefore provide avenues towards the improved collection of HSCs.

Online content

Any methods, additional references, Nature Research reporting summaries, source data, extended data, supplementary information, acknowledgements, peer review information; details of author contributions and competing interests; and statements of data and code availability are available at https://doi.org/10.1038/s41586-020-03057-y.

1. Gao, X., Xu, C., Asada, N. & Frenette, P. S. The hematopoietic stem cell niche: from embryo to adult. *Development* **145**, dev139691 (2018).
2. Hoggatt, J., Kfoury, Y. & Scadden, D. T. Hematopoietic stem cell niche in health and disease. *Annu. Rev. Pathol.* **11**, 555–581 (2016).
3. Katayama, Y. et al. Signals from the sympathetic nervous system regulate hematopoietic stem cell egress from bone marrow. *Cell* **124**, 407–421 (2006).
4. Lucas, D. et al. Chemotherapy-induced bone marrow nerve injury impairs hematopoietic regeneration. *Nat. Med.* **19**, 695–703 (2013).
5. Maryanovich, M. et al. Adrenergic nerve degeneration in bone marrow drives aging of the hematopoietic stem cell niche. *Nat. Med.* **24**, 782–791 (2018).
6. Méndez-Ferrer, S. et al. Mesenchymal and haematopoietic stem cells form a unique bone marrow niche. *Nature* **466**, 829–834 (2010).
7. Bensinger, W., DiPersio, J. F. & McCarty, J. M. Improving stem cell mobilization strategies: future directions. *Bone Marrow Transplant.* **43**, 181–195 (2009).
8. Ordovas-Montanes, J. et al. The regulation of immunological processes by peripheral neurons in homeostasis and disease. *Trends Immunol.* **36**, 578–604 (2015).
9. Pavlov, V. A., Chavan, S. S. & Tracey, K. J. Molecular and functional neuroscience in immunity. *Annu. Rev. Immunol.* **36**, 783–812 (2018).
10. Pinho-Ribeiro, F. A., Verri, W. A. & Chiu, I. M. Nociceptor sensory neuron–immune interactions in pain and inflammation. *Trends Immunol.* **38**, 5–19 (2017).
11. Tsunokuma, N. et al. Depletion of neural crest-derived cells leads to reduction in plasma noradrenaline and alters B lymphopoiesis. *J. Immunol.* **198**, 156–169 (2017).
12. Suekane, A. et al. CGRP–CRLR/RAMP1 signal is important for stress-induced hematopoiesis. *Sci. Rep.* **9**, 429 (2019).
13. Chow, A. et al. Bone marrow CD169$^+$ macrophages promote the retention of hematopoietic stem and progenitor cells in the mesenchymal stem cell niche. *J. Exp. Med.* **208**, 261–271 (2011).
14. Christopher, M. J., Rao, M., Liu, F., Woloszynek, J. R. & Link, D. C. Expression of the G-CSF receptor in monocytic cells is sufficient to mediate hematopoietic progenitor mobilization by G-CSF in mice. *J. Exp. Med.* **208**, 251–260 (2011).
15. Winkler, I. G. et al. Bone marrow macrophages maintain hematopoietic stem cell (HSC) niches and their depletion mobilizes HSCs. *Blood* **116**, 4815–4828 (2010).
16. Broxmeyer, H. E. et al. Rapid mobilization of murine and human hematopoietic stem and progenitor cells with AMD3100, a CXCR4 antagonist. *J. Exp. Med.* **201**, 1307–1318 (2005).
17. Lucas, D. et al. Norepinephrine reuptake inhibition promotes mobilization in mice: potential impact to rescue low stem cell yields. *Blood* **119**, 3962–3965 (2012).
18. Shastri, A. et al. Stimulation of adrenergic activity by desipramine enhances hematopoietic stem and progenitor cell mobilization along with G-CSF in multiple myeloma: A pilot study. *Am. J. Hematol.* **92**, 1047–1051 (2017).
19. Ford, C. D., Green, W., Warenski, S. & Petersen, F. B. Effect of prior chemotherapy on hematopoietic stem cell mobilization. *Bone Marrow Transplant.* **33**, 901–905 (2004).
20. Adams, G. B. et al. Haematopoietic stem cells depend on $G\alpha_s$-mediated signalling to engraft bone marrow. *Nature* **459**, 103–107 (2009).
21. Hagedorn, E. J., Durand, E. M., Fast, E. M. & Zon, L. I. Getting more for your marrow: boosting hematopoietic stem cell numbers with PGE2. *Exp Cell Res.* **329**, 220–226 (2014).
22. Hoggatt, J. et al. Differential stem- and progenitor-cell trafficking by prostaglandin E_2. *Nature* **495**, 365–369 (2013).
23. Sands, W. A. & Palmer, T. M. Regulating gene transcription in response to cyclic AMP elevation. *Cell. Signal.* **20**, 460–466 (2008).
24. Pulsipher, M. A. et al. Adverse events among 2408 unrelated donors of peripheral blood stem cells: results of a prospective trial from the National Marrow Donor Program. *Blood* **113**, 3604–3611 (2009).
25. Schweizerhof, M. et al. Hematopoietic colony-stimulating factors mediate tumor–nerve interactions and bone cancer pain. *Nat. Med.* **15**, 802–807 (2009).
26. Charles, A. & Pozo-Rosich, P. Targeting calcitonin gene-related peptide: a new era in migraine therapy. *Lancet* **394**, 1765–1774 (2019).
27. Cui, M., Gosu, V., Basith, S., Hong, S. & Choi, S. Polymodal transient receptor potential vanilloid type 1 nocisensor: structure, modulators, and therapeutic applications. *Adv. Protein Chem. Struct. Biol.* **104**, 81–125 (2016).
28. Asada, N. et al. Differential cytokine contributions of perivascular haematopoietic stem cell niches. *Nat. Cell Biol.* **19**, 214–223 (2017).

Methods

Data reporting

No statistical methods were used to predetermine sample size. The experiments were not randomized and the investigators were not blinded to allocation during experiments and outcome assessment.

Mice

$Na_v1.8$-Cre mice were a gift from J. Wood. $Na_v1.8$-Cre mice were bred with iDTA mice and iTdTomato mice (both from Jackson Laboratory) to generate $Na_v1.8$-Cre/iDTA nociceptor-deficient mice for functional studies and $Na_v1.8$-Cre/iTdTomato mice for imaging experiments, respectively. *Ramp1*$^{-/-}$ mice were generated in the 129S6/SvEv background[29]. All experiments with *Ramp1*$^{+/+}$ and *Ramp1*$^{-/-}$ mice were carried out using littermates by intercrossing *Ramp1*$^{+/-}$ heterozygous mice. *Carcrl*$^{fl/fl}$ mice were generated as previously described[30] and were bred with Vav1-iCre mice from Jackson Laboratory to conditionally delete *Calcrl* in haematopoietic cells. C57BL/6 CD45.1 and CD45.2 congenic mice were purchased from the Jackson Laboratory. Unless indicated otherwise, 8–10-week-old mice of both genders were used for experiments. All mice were maintained in pathogen-free conditions under a 12 h/12 h light/dark cycle, at a temperature of 21 ± 1 °C, a humidity of 40–70% and were fed with autoclaved food. This study complied with all ethical regulations involving experiments with mice, and all experimental procedures performed on mice were approved by the Animal Care and Use Committee of Albert Einstein College of Medicine.

Drug and chemical treatments

G-CSF was administered subcutaneously (s.c.) at a dose of 125 μg kg^{-1} twice a day (8 divided doses) beginning in the evening of the first day and blood was collected 3 h after the final morning dose. Newborn mice (2–4 days old) were injected s.c. with resiniferatoxin (RTX, Sigma-Aldrich, 50 μg kg^{-1}) and then three RTX escalating doses (30 μg kg^{-1}, 70 μg kg^{-1} and 100 μg kg^{-1}) were injected s.c. into 4-week-old mice on 3 consecutive days. Control littermates were injected with vehicle solution on the same days. For sympathetic nerve disruption in adults, 2 doses of 6OHDA or vehicle, 100 mg kg^{-1} on day 0, 250 mg kg^{-1} on day 2, were injected i.p. and analyses were performed on day 5. For steady-state experiments, CGRP (Sigma-Aldrich), substance P (GenScript) and isoproterenol (Sigma-Aldrich) were dosed at 14 μg per day, 5 μg per day and 40 μg per day, respectively, using s.c. implanted Alzet osmotic pumps (model 1007D). For mobilization experiments, CGRP (Tocris) was delivered into mice at 2.4 μg per day using Alzet osmotic pumps (model 1007D). Control animals were implanted with Alzet pumps containing saline (PBS; Gibco). Forskolin (Cayman Chemical) was given i.p. at a dose of 2.5 mg kg^{-1} twice a day (8 divided doses) at the same time as G-CSF treatment. For in vivo depletion of macrophages, clodronate liposomes or PBS liposome as control (250 μL) were infused i.v. one week before analysis. For chemotherapy treatment, mice were injected with cisplatin (10 mg kg^{-1} once per week; Teva) for 5 weeks, and were allowed to recover for 6–8 weeks before the experiment. Desipramine (Tocris, 10 mg kg^{-1} i.p.) or saline (as control) treatment was started 4 days before G-CSF injection and continued throughout the experiment. For AMD3100-induced mobilization, mice received a single dose of AMD3100 (Sigma, 5 mg kg^{-1}, i.p.) 3 h before blood collection. C57BL/6 wild-type mice were fed with a capsaicin-containing diet (100 ppm, 100 mg kg^{-1}) or a control diet from a week before G-CSF administration and until analysis.

Bone marrow transplantation assays

Competitive repopulation assays were performed using the CD45.1/CD45.2 congenic system. CD45.1 recipient mice were lethally irradiated (12 Gy, two split doses) in a Cesium Mark 1 irradiator (JL Shepherd & Associates). For competitive repopulation assays, 0.5×10^6 donor bone marrow cells (CD45.2) or 50 μl of mobilized blood (CD45.2) were transplanted together with 0.5×10^6 CD45.1 competitor bone marrow cells into lethally irradiated CD45.1 recipients. For competitive HSC repopulation assays, 250 donor HSCs (CD45.2) were sorted from mobilized blood and transplanted together with 0.5×10^6 CD45.1 competitor bone marrow cells into lethally irradiated CD45.1 recipients. CD45.1/CD45.2 chimerism of recipient blood and bone marrow was analysed up to 16 or 20 weeks after transplantation by fluorescence-activated cell sorting (FACS). For RAMP1 reciprocal bone marrow transplantation, 2×10^6 donor bone marrow cells from *Ramp1*$^{+/+}$ or *Ramp1*$^{-/-}$ mice were transplanted into lethally irradiated *Ramp1*$^{+/+}$ or *Ramp1*$^{-/-}$ recipient mice (12 Gy, two split doses). For the mixed chimaera experiment, 10^6 CD45.1 bone marrow cells from C57BL/6 wild-type mice were mixed with 10^6 CD45.2 bone marrow cells (1:1 ratio) from *Ramp1*$^{+/+}$ or *Ramp1*$^{-/-}$ mice and transplanted into lethally irradiated CD45.1 recipient mice (12 Gy, two split doses). For the G-CSF-induced mobilization experiment with Vav1-iCre mice, 2×10^6 donor bone marrow cells from Vav1-iCre$^+$;*Calcrl*$^{w/w}$ or Vav1-iCre$^+$;*Calcrl*$^{fl/fl}$ mice were transplanted into lethally irradiated CD45.1 recipient mice (12 Gy, two split doses). G-CSF was administrated to induce mobilization in recipient mice at least 8 weeks after transplantation.

Bone marrow homing assay

Donor bone marrow cells were collected from PBS-, RTX/6OHDA-treated mice (CD45.2), *Ramp1*$^{+/+}$ or *Ramp1*$^{-/-}$ mice (CD45.2) and injected (5×10^6 cells) into lethally irradiated wild-type mice (CD45.1, 12 Gy, single dose). Sixteen hours after irradiation and injection, the recipient bone marrow was collected (femurs, tibiae, humeri and pelvis) to determine the number of homed donor HSCs and LSK cells using FACS analysis. The homing efficiency was determined by dividing the absolute numbers of homed HSCs or LSK cells in bone marrow by the absolute numbers of injected HSCs or LSKs (input).

CFU-C assay

The haematopoietic progenitor colony-forming units in culture (CFU-C) assay was assayed by plating RBC-lysed peripheral blood into methylcellulose (Stem Cell Technologies, cat. no. 3434). Cultures were plated in 35 mm culture dishes and incubated for 7 days in humid chambers before colonies were scored.

Transwell migration assay

Femurs, tibiae and humeri from C57BL/6 wild-type mice were flushed with 1 ml of phosphate-buffered saline (PBS, Corning) in a syringe with a 21-gauge needle, erythrocytes were lysed, and lineage-positive cells were immunomagnetically depleted from the bone marrow cells using a biotinylated lineage antibody cocktail (CD3e, B220, CD11b, Ter119 and Gr-1, at 1:100 dilution; BD Bioscience 559971) followed by streptavidin magnetic beads (Miltenyi Biotech 130-48-101). Lineage-depleted bone marrow cells were transferred into the 6.5 mm transwell plates (Corning 3421) containing alpha MEM (Gibco) supplemented with 10% FBS (Stem Cell Technologies) and the bottoms of transwells were filled with medium containing 100 ng ml^{-1} CXCL12 (Peprotech). Transwell plates were incubated at 37 °C for 3 h and migrated cells in the bottom wells were then plated in CFU-C as described in the previous section.

Flow cytometry and sorting

Peripheral blood was collected by retro-orbital bleeding of mice anaesthetized with isoflurane and was collected in polypropylene tubes containing EDTA. Blood parameters were determined with the Advia120 Hematology System (Siemens). Bone marrow cells were obtained by flushing and dissociating using a 1-ml syringe with PBS via a 21-gauge needle. For analysis of stromal and endothelial cell populations, intact flushed bone marrow plugs were digested at 37 °C for 30 min in 1 mg ml^{-1} collagenase type IV (Gibco), 2 mg ml^{-1} Dispase (Gibco) and 500 μg ml^{-1} DNase I (Sigma-Aldrich) in Hank's balanced salt solution (HBSS, Gibco). For FACS analysis and sorting, red blood cells were lysed and

washed in ice-cold PEB (PBS containing 0.5% BSA and 2 mM EDTA) before staining with antibodies in PEB. The following antibodies were used for FACS: the anti-lineage panel cocktail (CD3e, B220, CD11b, Ter119 and Gr-1, at 1:100 dilution) was from BD Bioscience (559971), anti-Sca-1-FITC (D7; 11-5981-85), anti-CD117(c-Kit)-PE/Cy7 (2B8; 105814), anti-CD48-PerCP-eFluor710 (HM48-1; 46-0481-85), anti-CD150-PE (TC15-12F12.2; 115904), anti-B220-APC-eFluor780 (RA3-6B2; 47-0452-82), anti-CD3e-PerCP-Cy5.5 (145-2C11; 45-0031-82), anti-Gr-1-FITC (RB6-8C5; 11-5931-85), anti-CD11b-PE (M1/17; 12-0112-83), anti-CD45.1-PE/Cy (A20; 25-0453-82), anti-CD45.2-FITC (104; 109806), anti-Sca-1-APC (D7; 17-5981-83), anti-CD117-BV421 (2B8; 105828), anti-CD45-PerCP-Cy5.5 (30-F11, 45-0451-82), anti-Ter119-PerCP-Cy5.5 (TER-119; 45-5921-82), anti-CD31-PE/Cy7 (390; 25-0311-82), anti-CD51-PE (RMV-7; 12-0512-83), anti-PDGFRα(CD140α)-APC (APA5; 17-1401-81), anti-Gr-1-APC (RB6-8C5; 17-5931-82), anti-F4/80-PE (BM8; 123110), anti-CD115-PE/C7 (AFS98; 25-1152-82), streptavidin APC-eFluor 780 (47-4317-82), anti-CXCR4-AF647 (L276F12, 146504), anti-CD49d-APC (R1-2, 17-0492-82), anti-CD44-APC (IM7, 17-0441-82), all purchased from BioLegend or eBioscience. Unless otherwise specified, all antibodies were used at a 1:100 dilution. The cell cycle was analysed with Ki67 and Hoechst 33342 (Sigma) . FACS analyses were carried out using BD LSRII flow cytometry (BD Biosciences) and cell sorting experiments were performed using a MoFlo Astrios (Beckman Coulter). Data were analysed with FlowJo 10.4.0 (LCC) and FACS Diva 6.1 software (BD Biosciences).

Immunofluorescence imaging

Anti-CD31-Alexa Fluor 647 (MEC13.3, 102516, BioLegend) and anti-CD144 (VE-Cadherin)-Alexa Fluor 647 (BV13, 138006, BioLegend) (7.5 µg each) were injected i.v. into mice, and mice were perfusion-fixed with 4% paraformaldehyde (PFA) 10 min after the injection. Bones were post-fixed with 4% PFA for another 15 min at room temperature. For cryopreservation, the bones were incubated sequentially in 15% sucrose/PBS at 4 °C overnight and in 30% sucrose/PBS at room temperature for 2 h, and embedded and flash-frozen in SCEM embedding medium (Section-Lab). Frozen sections were prepared (20-µm thick) with a Cryostat (CM3050, Leica) using Kawamoto's tape transfer method. For immunofluorescence staining, sections were rinsed with PBS, post-fixed with 4% PFA for 30 min followed by blocking with 20% donkey serum (Sigma) in 0.5% Triton X-100/PBS for 2 h at room temperature. The following primary antibodies were used for nerve staining: anti-tyrosine hydroxylase (TH) antibody (AB152, Millipore), anti-CGRP (ab36001, Abcam) and anti-TUBB3-Alexa Fluor 488 (657404), used at 1:100 (TH and TUBB3) or 1:1,000 (CGRP) dilution in 2% donkey serum with 0.1% Triton X-100/PBS for 48–72 h at 4 °C. Primary antibody staining experiments were washed three times with PBS, and incubated with secondary antibodies (1:200 dilution in 2% donkey serum with 0.1% Triton X-100/PBS) at room temperature for 1 h. The secondary antibodies used were as follows: donkey anti-rabbit IgG BV421 (406410, BioLegend), donkey anti-goat IgG AF568 (A11057, Invitrogen), donkey anti-rabbit IgG AF488 (A21206, Invitrogen), donkey anti-goat IgG AF488 (A11055, Invitrogen). All images were acquired at room temperature using a Zeiss Axio examiner D1 microscope (Zeiss) with confocal scanner unit (Yokogawa). For quantification of nerve fibres, *z*-stack images were stitched together and reconstructed using Slide Book Software 6.0 (Intelligent Imaging Innovations). Nerve densities were quantified by total length or total area (as indicated in the figure legends) of nerve fibres divided by the bone marrow area from 8–20 *z*-stack projections per mouse and 3–5 mice per group (each data point on the graphs represents one mouse).

RNA isolation and quantitative real-time PCR

RNA was isolated according to the manufacturer's instructions using Dynabeads mRNA DIRECT Purification Kit (61012, Invitrogen). Conventional reverse transcription, using the RNA to cDNA EcoDry Premix (639549, Takara), was performed in accordance with the manufacturer's instructions. Quantitative real-time PCR was performed with SYBR Green on QuantStudio 6 Flex Real-Time PCR System (Applied Biosystem, Thermo Fisher). The sequences of the oligonucleotides used can be provided upon reasonable request to the corresponding author.

RNA sequencing analysis

Total RNA from 2,000 sorted HSCs was extracted using the RNeasy Plus Micro kit (Qiagen), and assayed for integrity and purity using an Agilent 2100 Bioanalyzer (Agilent Technologies). RNA sequencing data generated from Illumina Platform PE150 were processed using the following pipeline. In brief, paired-end sequencing reads were aligned to the mouse genome using Spliced Transcripts Alignment to a Reference (STAR) v.2.6.1. Alignments were parsed using the program TopHat. HTSeq v.0.6.1 was used to count the read numbers mapped of each gene, and then the fragments per kilobase of exon model per million mapped reads (FPKM) of each gene was calculated on the basis of the length of the gene and reads count mapped to this gene. Differential expression analysis between two groups was performed using the DESeq2 R package, which provides statistical routines for determining differential expression in digital gene expression data using a model based on the negative binomial distribution. The resulting *P* values were adjusted using the Benjamini–Hochberg approach for controlling the false discovery rate.

ELISA

Mouse CXCL12/SDF-1 alpha Quantikine ELISA Kit was purchased from R&D (MCX120) and used according to the manufacturer's instructions. CGRP EIA Kit was purchased from Cayman Chemical (589001) and used according to the manufacturer's instructions. All bone marrow extracellular fluid used for ELISA was collected by flushing the bone marrow of one or two femurs into 500 µl PBS and subsequently pelleting the cells by centrifugation. The resulting supernatant was removed from the cell pellet and frozen at −80 °C for analysis.

Quantification and statistical analysis

All data are presented as mean ± s.e.m. *n* represents the number of mice in each experiment, as detailed in the figure legends. Statistical significance was determined by an unpaired, two-tailed Student's *t*-test to compare two groups or a one-way ANOVA for multiple group comparisons. Statistical analyses were performed and data presented using GraphPad Prism 8 (GraphPad Software), FACS Diva 6.1 software (BD Biosciences, FlowJo 10.4.0 (LLC), Slide Book Software 6.0 (Intelligent Imaging Innovations) and QuantStudio 6 Real-Time PCR Software (Applied Biosystem, Thermo Fisher).

Reporting summary

Further information on research design is available in the Nature Research Reporting Summary linked to this paper.

Data availability

RNA sequencing data have been deposited in the Gene Expression Omnibus under accession number GSE156449. All other data are available from the corresponding author upon reasonable request. Source data are provided with this paper.

29. Li, M. et al. Deficiency of RAMP1 attenuates antigen-induced airway hyperresponsiveness in mice. *PLoS ONE* **9**, e102356 (2014).
30. Fritz-Six, K. L., Dunworth, W. P., Li, M. & Caron, K. M. Adrenomedullin signaling is necessary for murine lymphatic vascular development. *J. Clin. Invest.* **118**, 40–50 (2008).

Acknowledgements We thank J. Wood for providing Na$_v$1.8-Cre mice, C. Prophete for technical assistance, A. Birbrair and N. Asada for advice with the initial experiments, and D. Sun from the Human Stem Cell FACS and Xenotransplantation Facility for assistance with cell sorting. This work was supported by grants from the National Institutes of Health (U01DK116312, R01DK056638, R01DK112976 and R01HL069438) to P.S.F. H.L. is the recipient of a F32 Ruth L. Kirschstein Postdoctoral Individual National Research Service Award (HL142243-01).

Author contributions X.G. designed the study, performed most of the experiments, analysed data and wrote the manuscript. D.Z. advised on experiment design, helped with flow cytometry analysis, sorting and bone marrow transplantations, and provided input on the manuscript. C.X. participated in study design and performed experiments. H.L. advised on experiment design and helped with experiments. K.M.C. provided *Ramp1*$^{-/-}$ and *Calcrl*$^{fl/fl}$ mice and commented on the manuscript. P.S.F. designed and supervised the study, interpreted data and wrote the manuscript.

Competing interests P.S.F. serves as consultant for Pfizer, has received research funding from Ironwood Pharmaceuticals and is a shareholder of Cygnal Therapeutics. The rest of the authors declare no competing interests.

Additional information

Supplementary information is available for this paper at https://doi.org/10.1038/s41586-020-03057-y.

Correspondence and requests for materials should be addressed to P.S.F.

Peer review information *Nature* thanks Iannis Aifantis, Toshio Suda and the other, anonymous, reviewer(s) for their contribution to the peer review of this work.

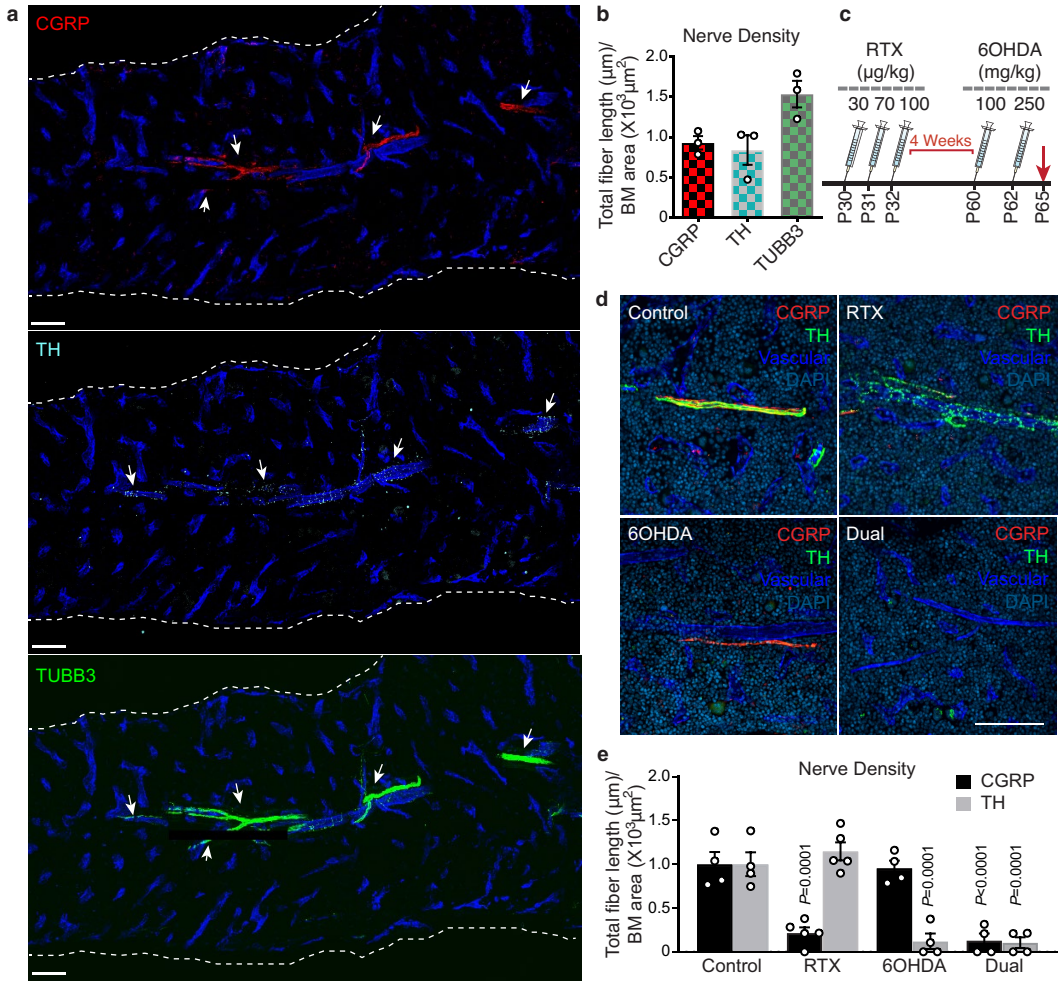

Extended Data Fig. 1 | Characterization of nociceptive and sympathetic innervation in the bone marrow. a, **b**, Representative confocal *z*-stack projection montages of C57BL/6 mouse femur stained for CGRP (nociceptive nerves), TH (sympathetic nerves), and TUBB3 (all peripheral nerves), $CD31^+CD144^+$ double-positive vasculature. Scale bar, 100 μm. Femoral sensory and sympathetic innervation is quantified by the total length of all $CGRP^+$, TH^+ or $TUBB^+$ nerve fibres divided by the bone marrow (BM) area. $n = 3$ mice. **c**, Schematic illustration of the pharmacological denervation experiment using RTX and 6OHDA. **d**, **e**, Representative images of confocal *z*-stack projections from femurs of control, RTX-, 6OHDA- and dual-denervated mice stained for $CGRP^+$ nociceptive nerve fibres, TH^+ sympathetic nerve fibres, $CD31^+CD144^+$ blood vessels and DAPI. Scale bar, 100 μm. Femoral sensory and sympathetic innervation is quantified by the total length of $CGRP^+$ or TH^+ nerves divided by total bone marrow area. Data from $n = 4, 5, 4, 4$ mice, respectively. Data are mean ± s.e.m.; significance was assessed using a one-way ANOVA.

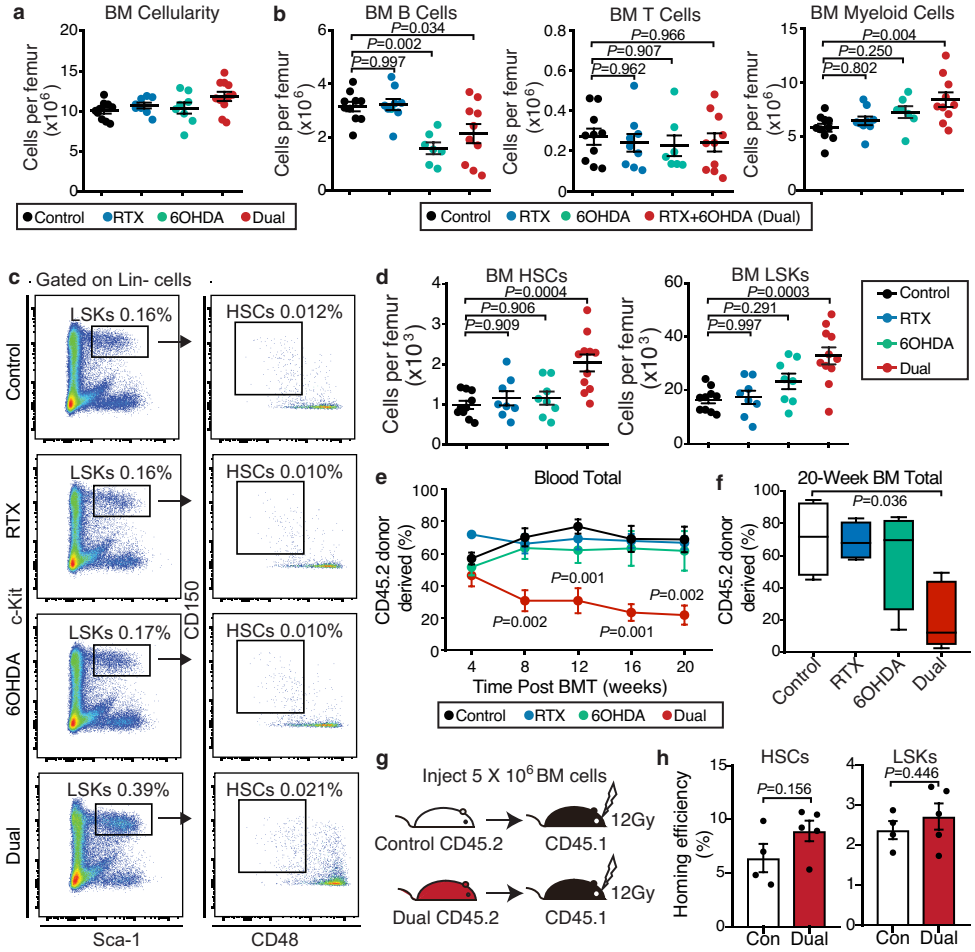

Extended Data Fig. 2 | Nociceptive or sympathetic nerves are dispensable for HSC maintenance, whereas the depletion of both systems expands poorly functional HSCs. a, **b**, Bone marrow cellularity and absolute numbers of B cells ($B220^+$), T cells ($CD3e^+$) and myeloid cells ($Mac\text{-}1^+$) per femur from control, RTX, 6OHDA, or dual-denervated mice. $n = 10, 8, 8, 11$ (**a**) and $10, 9, 7, 10$ (**b**) mice, respectively. **c**, Representative FACS plots showing the gating strategy for $Lin^-Sca\text{-}1^+Kit^+CD150^+CD48^-$ HSCs. The same gating strategy was used throughout. **d**, Absolute number of HSCs and LSK cells ($Lin^-Sca\text{-}1^+Kit^+$) per femur from control, RTX, 6OHDA or dual-denervated mice. $n = 10, 8, 8, 11$ mice, respectively. **e**, Peripheral blood chimerism ($CD45.2^+$) in CD45.1-recipient mice transplanted with 0.5×10^6 CD45.1 competitor bone marrow cells mixed with 0.5×10^6 donor bone marrow cells (CD45.2) from control, RTX, 6OHDA or dual-denervated mice at the indicated time points post-transplantation. $n = 4, 4, 4, 5$ mice, respectively. **f**, Bone marrow chimerism ($CD45.2^+$) 20 weeks after transplantation. **g**, Experimental design to determine the homing efficiency of HSCs and LSK cells (CD45.2) from control- or dual-denervated mice to the bone marrow of recipients (CD45.1). **h**, Homing efficiency of donor CD45.2 HSCs and LSK cells detected in the recipient bone marrow. $n = 4, 5$ mice, respectively. Data are mean ± s.e.m.; significance was assessed using a two-tailed unpaired Student's *t*-test (**h**) or one-way ANOVA (**a**, **b**, **d**–**f**). For box plots, the box spans from the 25th to 75th percentiles and the centre line was plotted at the median. Whiskers represent minimum to maximum range.

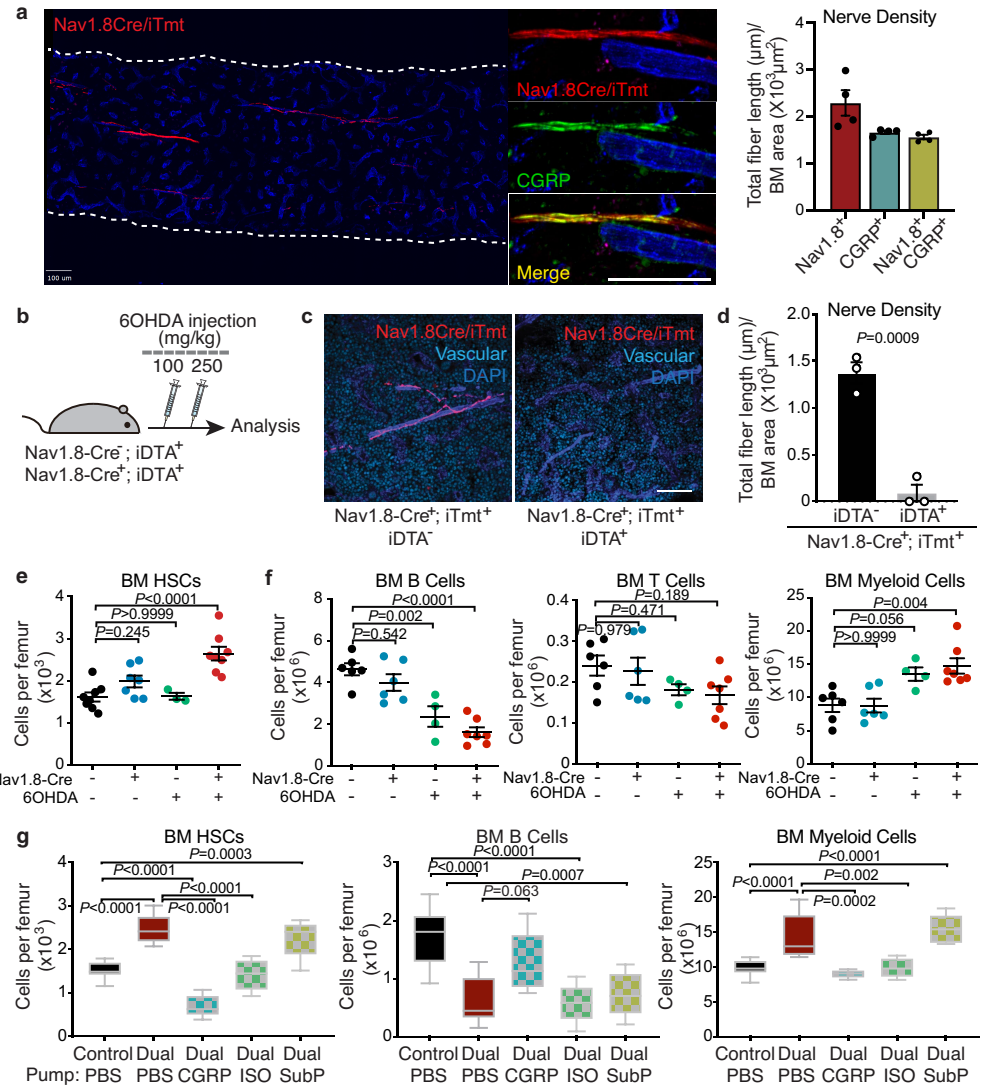

Extended Data Fig. 3 | Expansion of phenotypic HSCs after dual sympathetic and nociceptive denervation is normalized by administration of CGRP or a β-adrenergic agonist. a, Representative confocal *z*-stack projections from femurs of $Na_v1.8$-Cre$^+$; iTdTomato$^+$ mice stained for CD31$^+$CD144$^+$ vasculature and CGRP$^+$ nociceptive nerves. Nociceptive innervation quantified by the total length of all $Na_v1.8^+$ (red), CGRP$^+$ (green) and $Na_v1.8^+$CGRP$^+$ double positive (yellow) nerves divided by the bone marrow area. $n = 4$ mice. **b**, Schematic illustration of the dual denervation experiment with $Na_v1.8$-Cre; iDTA mice. **c**, **d**, Representative images of confocal *z*-stack projections from femurs of $Na_v1.8$-Cre$^+$;iTdTomato$^+$;iDTA$^-$ or $Na_v1.8$-Cre$^+$; iTdTomato$^+$;iDTA$^+$ mice stained for blood vessels (blue). Quantification of TdTomato$^+$ nociceptive nerves in the femurs. $n = 3$ mice per group. **e**, **f**, Absolute numbers of HSCs (Lin$^-$Sca-1$^+$Kit$^+$CD150$^+$CD48$^-$), B cells (B220$^+$), T cells (CD3e$^+$) and myeloid cells (Mac-1$^+$) per femur from $Na_v1.8$-Cre$^-$;iDTA$^+$ or $Na_v1.8$-Cre$^+$; iDTA$^+$ mice with or without 6OHDA treatment. Each dot represents data from individual mice. $n = 8, 7, 3, 8$ (**e**) and 6, 6, 4, 7 (**f**) mice, respectively. **g**, Absolute numbers of HSCs, B cells and myeloid cells per femur from control and dual-denervated mice implanted with osmotic pumps containing saline as control, CGRP, isoproterenol or substance P. $n = 14, 9, 5, 5, 5$ mice respectively. Data are mean ± s.e.m. Significance was assessed using a two-tailed unpaired Student's *t*-test (**d**) or one-way ANOVA (**e**–**g**). For box plots, the box spans from the 25th to 75th percentiles and the centre line was plotted at the median. Whiskers represent minimum to maximum range.

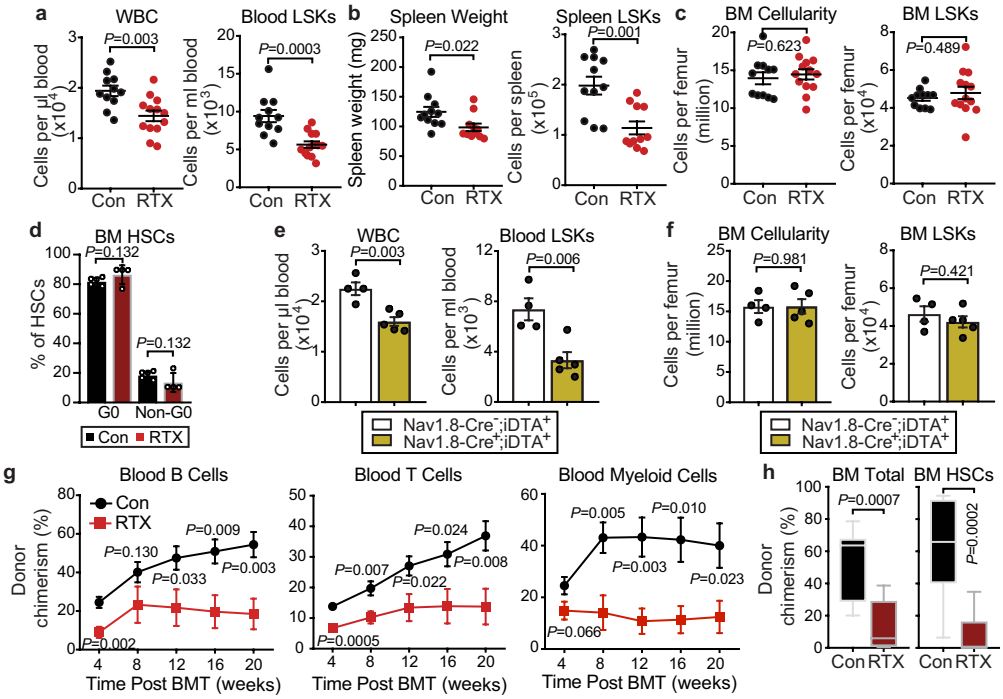

Extended Data Fig. 4 | G-CSF-induced HSPC mobilization is impaired in mice that lack nociceptor neurons. a, White blood cell counts and absolute numbers of LSK cells per ml of peripheral blood after G-CSF mobilization in vehicle-treated control and RTX-treated mice. $n = 11, 13$ mice, respectively. **b**, Spleen weight and the absolute numbers of LSK cells in the spleen after G-CSF mobilization in vehicle-treated control and RTX-treated mice. $n = 11$ mice per group. **c**, Bone marrow cellularity and the absolute numbers of LSK cells in the bone marrow after G-CSF-induced mobilization in vehicle-treated control and RTX-treated mice. $n = 11, 13$ mice, respectively. **d**, Cell cycle analysis of bone marrow HSCs ($Lin^-Sca\text{-}1^+Kit^+CD150^+CD48^-$) from control or RTX-treated mice determined by FACS using anti-Ki67 and Hoechst 33342 staining. $n = 6, 4$ mice, respectively. **e**, White blood cell counts and absolute numbers of LSK cells per ml of peripheral blood after G-CSF-induced mobilization in $Na_v1.8\text{-}Cre^-;iDTA^+$ and $Na_v1.8\text{-}Cre^+;iDTA^+$ mice. $n = 4, 5$ mice, respectively. **f**, Bone marrow cellularity and the absolute numbers of LSK cells in the bone marrow after G-CSF-induced mobilization in $Na_v1.8\text{-}Cre^-;iDTA^+$ and $Na_v1.8\text{-}Cre^+;iDTA^+$ mice. $n = 4, 5$ mice, respectively. **g**, Peripheral blood B-cell ($B220^+CD45.2^+$), blood T-cell ($CD3e^+CD45.2^+$), and myeloid-cell ($Mac\text{-}1^+CD45.2^+$) donor chimerism in CD45.1-recipient mice transplanted with mobilized blood (CD45.2) derived from saline or RTX-treated mice mixed with CD45.1 competitor bone marrow cells at the indicated time points post-transplantation. $n = 9, 8$ mice, respectively. **h**, Total bone marrow chimerism ($CD45.2^+$) and bone marrow HSC chimerism ($Lin^-Sca\text{-}1^+Kit^+CD150^+CD48^-CD45.2^+$) 20 weeks after transplantation. $n = 9, 8$ mice, respectively. Data are mean ± s.e.m. Significance was assessed using a two-tailed unpaired Student's *t*-test. For box plots, the box spans from the 25th to 75th percentiles and the centre line was plotted at the median. Whiskers represent minimum to maximum range.

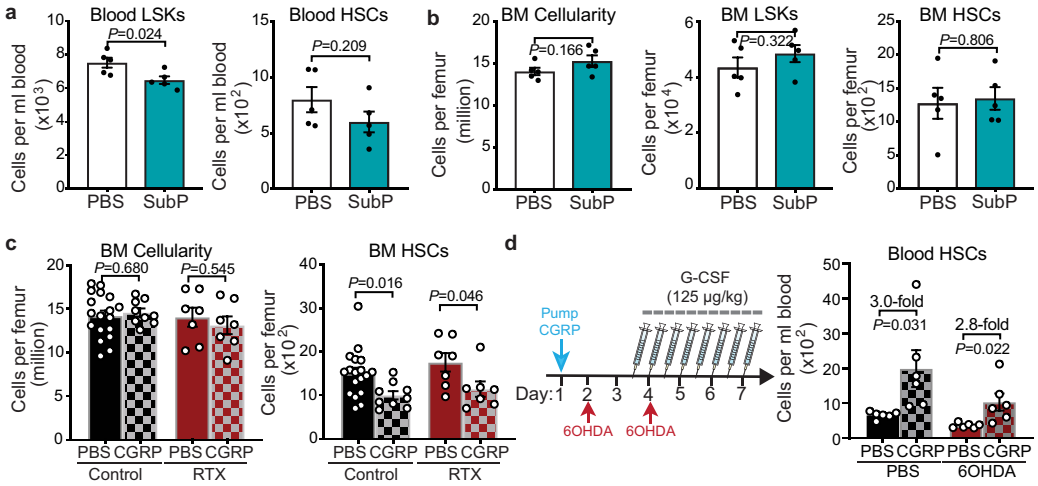

Extended Data Fig. 5 | The neuropeptide CGRP, but not substance P, promotes G-CSF-induced HSC mobilization. a, Absolute numbers of HSCs ($Lin^-Sca\text{-}1^+Kit^+CD150^+CD48^-$) and LSK cells ($Lin^-Sca\text{-}1^+Kit^+$) per ml of peripheral blood after G-CSF-induced mobilization in C57BL/6 mice implanted with osmotic pumps containing saline or substance P. $n = 5$ mice per group. **b**, Bone marrow cellularity and the absolute numbers of LSK cells and HSCs in the bone marrow after G-CSF administration in C57BL/6 mice implanted with osmotic pumps containing saline or substance P. $n = 5$ mice per group. **c**, Bone marrow cellularity and the absolute numbers of HSCs per femur from mice described in Fig. 2a. $n = 18, 9, 7, 7$ mice, respectively. **d**, Left, experimental design to determine the effect of CGRP on HSC mobilization of 6OHDA-denervated mice. Right, absolute number of HSCs per ml of peripheral blood after G-CSF administration in saline-or 6OHDA- treated C57BL/6 mice implanted with osmotic pumps containing saline or CGRP. $n = 6$ mice per group. Data are mean ± s.e.m.; significance was assessed using a two-tailed unpaired Student's *t*-test.

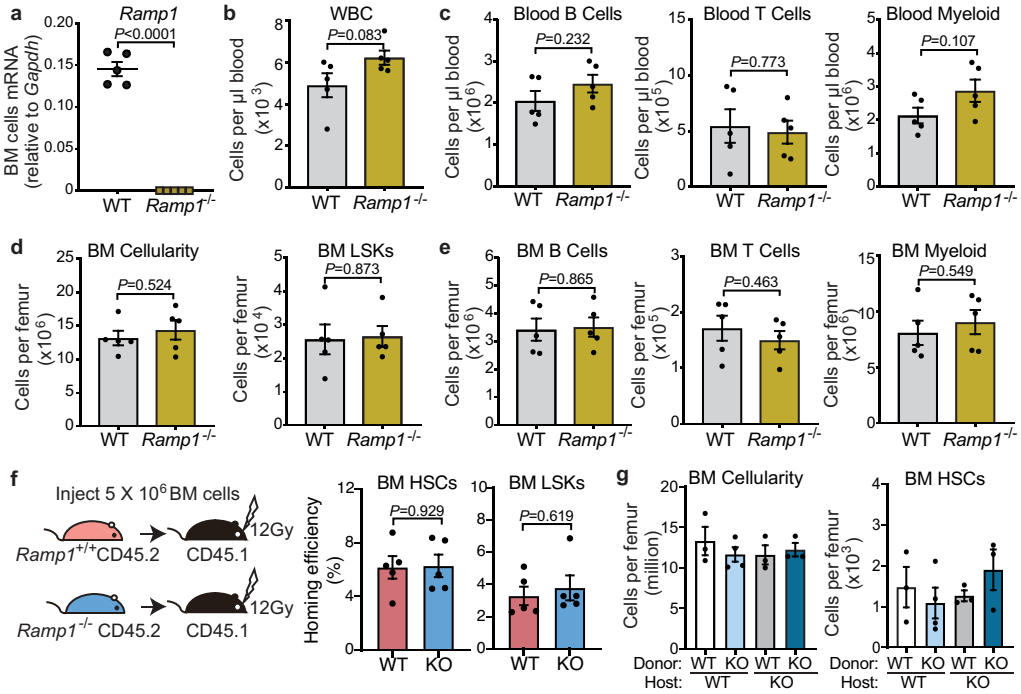

Extended Data Fig. 6 | *Ramp1*-deficient mice exhibit no haematopoietic defect at steady state. a, *Ramp1* mRNA expression levels determined by quantitative PCR in total bone marrow cells derived from *Ramp1*$^{+/+}$ or *Ramp1*$^{-/-}$ mice. $n = 5$ biological samples. **b**, **c**, White blood cell counts (**b**) and the absolute numbers of B cells (B220$^+$), T cells (CD3e$^+$) and myeloid cells (Mac-1$^+$) (**c**) per ml of peripheral blood from *Ramp1*$^{+/+}$ or *Ramp1*$^{-/-}$ mice at steady state. $n = 5$ mice per group. **d**, **e**, Bone marrow cellularity (**d**) and the absolute numbers of LSK cells, B cells (B220$^+$), T cells (CD3e$^+$) and myeloid cells (Mac-1$^+$) (**e**) per femur from *Ramp1*$^{+/+}$ or *Ramp1*$^{-/-}$ mice at steady state. $n = 5$ mice per group. **f**, Left, experimental design to determine the homing efficiency of HSCs (Lin$^-$ Sca-1$^+$Kit$^+$CD150$^+$CD48$^-$) and LSK cells from *Ramp1*$^{+/+}$ and *Ramp1*$^{-/-}$ mice (CD45.2) to the bone marrow of lethally irradiated recipients (CD45.1). Right, the percentage of donor CD45.2$^+$ HSCs and LSK cells detected in the recipient bone marrow. $n = 5$ mice per group. **g**, Bone marrow cellularity and the absolute number of HSCs in the bone marrow. $n = 3, 4, 3, 3$ mice, respectively. Data are mean ± s.e.m. Significance was assessed using a two-tailed unpaired Student's *t*-test (**a**–**f**) or one-way ANOVA (**g**).

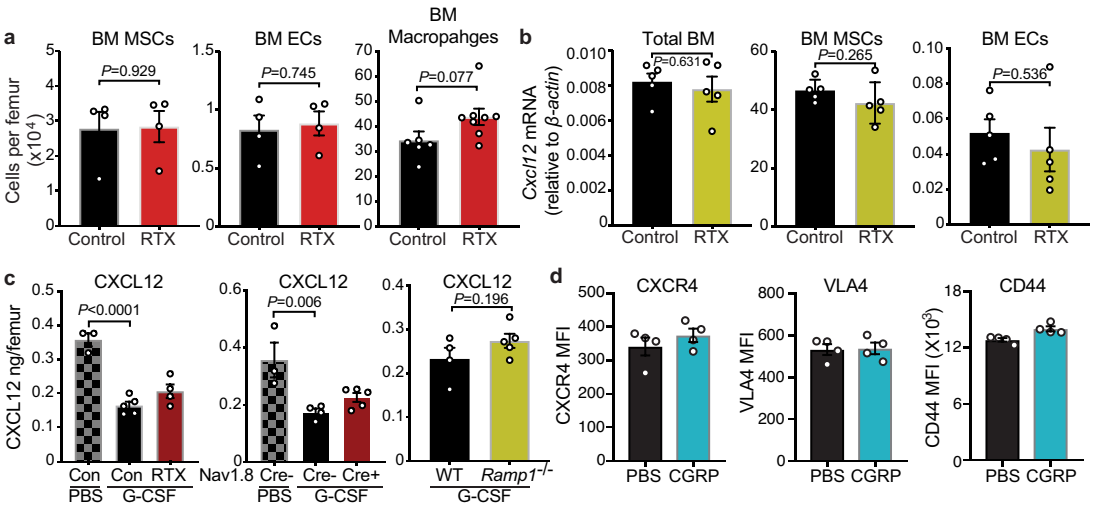

Extended Data Fig. 7 | Nociceptive-nerve-deficient mice exhibit no alteration of HSC niche components after G-CSF treatment. a, Absolute numbers of mesenchymal stem cells (MSCs) ($CD45^-Ter119^-CD31^-CD51^+PDGFR\alpha^+$), endothelial cells (ECs) ($CD45^-Ter119^-CD31^{high}$) and macrophages ($Gr\text{-}1^-F4/80^+CD115^{int}SSC^{int/low}$) per femur from saline- or RTX-treated mice after G-CSF treatment. $n = 4, 4$ (left and middle), 6, 8 (right) mice, respectively. **b**, qPCR quantification of *Cxcl12* mRNA levels in total bone marrow cells, sorted MSCs and ECs from saline- or RTX-treated mice after G-CSF treatment. $n = 5$ mice per group. **c**, Levels of CXCL12 in bone marrow extracellular fluid (BMEF) measured by ELISA. $n = 3, 5, 4$ (left), 3, 4, 5 (middle), 4, 5 (right) mice. **d**, Mean fluorescence intensities (MFI) in the expression of CXCR4, VLA4 and CD44 on HSCs ($Lin^-Sca\text{-}1^+Kit^+CD150^+CD48^-$). $n = 4$ mice per group. Data are mean ± s.e.m. Significance was assessed using a two-tailed unpaired Student's *t*-test (**a**, **b**, **d**) or one-way ANOVA (**c**).

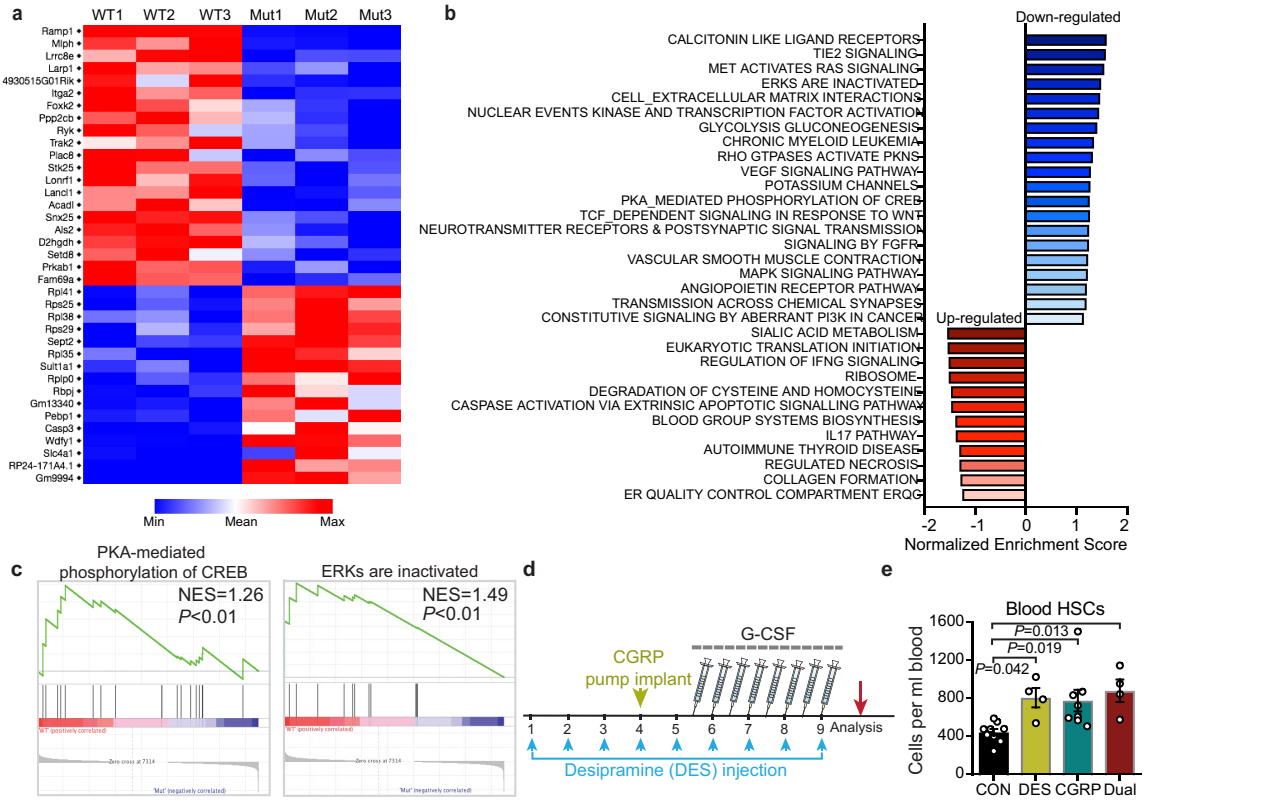

Extended Data Fig. 8 | Transcriptome analysis by RNA sequencing of HSCs from *Ramp1*$^{+/+}$ and *Ramp1*$^{-/-}$ mice. a, Heat map shows differentially expressed genes between wild-type- and *Ramp1*$^{-/-}$-sorted HSCs (adjusted *P* value <0.05). **b**, Gene set enrichment analyses showing upregulated and downregulated pathways in *Ramp1*$^{-/-}$ HSCs compared to wild-type HSCs ($P < 0.01$, $n = 3$ biological replicates per group). **c**, Gene set enrichment analyses showing significant alterations of gene sets involved in the $G\alpha_s$/adenylyl cyclase/cAMP pathway. **d**, Schematic illustration of the dual stimulation experiment. **e**, Absolute number of HSCs ($Lin^-Sca\text{-}1^+Kit^+CD150^+CD48^-$) in the mobilized peripheral blood of mice treated with control saline, desipramine (DES), CGRP, or both DES and CGRP. $n = 9, 4, 8, 4$ mice, respectively. Data are mean ± s.e.m. Significance was assessed using a one-way ANOVA.

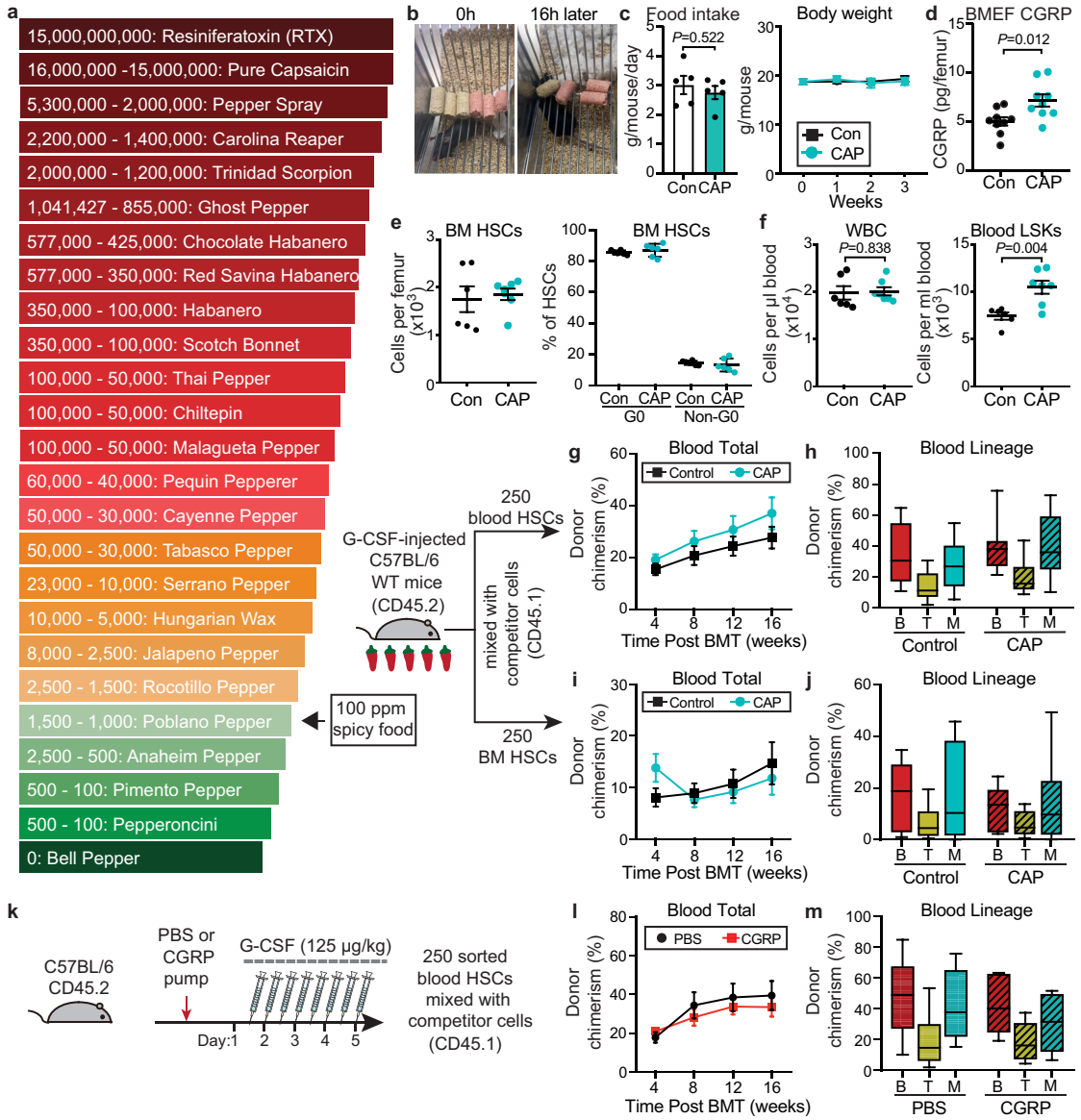

Extended Data Fig. 9 | Ingestion of spicy food enhances HSC mobilization. **a**, Scoville heat scale for chili peppers. 100 ppm = 100 mg kg^{-1}. **b**, Three pellets of standard chow (brown) and three pellets of spicy chow (red) were provided to two mice at 18:00 on day 1. Sixteen hours later (10:00 on day 2), two of the three standard pellets had been consumed whereas the spicy food pellets remained untouched. **c**, Daily food intake (left) and the body weight (right) of mice fed with standard diet or capsaicin-containing diet. $n = 5$ (left), 4 mice (right) per group. **d**, CGRP levels in the BMEF from mice fed with control diet or capsaicin diet. $n = 9$ mice per group. **e**, Left, absolute numbers of HSCs (Lin$^-$ Sca-1$^+$Kit$^+$CD150$^+$CD48$^-$) in the bone marrow after G-CSF-induced mobilization in mice fed with standard or capsaicin-containing chow. $n = 6, 7$ mice, respectively. Right, cell cycle analysis of bone marrow HSCs was determined by FACS using anti-Ki67 and Hoechst 33342 staining. $n = 6$ mice. **f**, White blood cell (WBC) counts (left) and absolute numbers of LSK cells (right) per ml of peripheral blood after G-CSF-induced mobilization in mice fed with standard diet or capsaicin-containing diet. $n = 6, 7$ mice, respectively. **g**, **i**, Peripheral total blood donor chimerism (CD45.2$^+$) in CD45.1-recipient mice transplanted with 0.5×10^6 CD45.1 competitor bone marrow cells and 250 HSCs sorted from mobilized blood (**g**) or bone marrow (**i**) from mice fed with standard or capsaicin chow. $n = 9, 8$ (**g**), 8, 8 (**i**) mice, respectively. **h**, **j**, Peripheral blood B cell (B220$^+$CD45.2$^+$), T cell (CD3e$^+$CD45.2$^+$) and myeloid cell (Mac-1$^+$CD45.2$^+$) donor chimerism in CD45.1-recipient mice transplanted with 250 blood HSCs (**h**) or bone marrow HSCs (**j**) with competitor bone marrow cells at 16 weeks post-transplantation. $n = 9, 8$ (**h**), 8, 8 (**j**) mice, respectively. **k**, Experimental design to determine the effects of CGRP administration on HSC competitiveness. **l**, Peripheral total blood donor chimerism (CD45.2$^+$) in CD45.1-recipient mice transplanted with 0.5×10^6 CD45.1 competitor bone marrow cells and 250 HSCs sorted from mobilized blood from PBS- or CGRP-treated mice. $n = 7, 9$ mice, respectively. **m**, Peripheral blood B cell, T cell and myeloid cell donor chimerism in CD45.1-recipient mice transplanted with 250 blood HSCs with competitor bone marrow cells at 16 weeks post-transplantation. $n = 7, 9$ mice, respectively. Data are mean ± s.e.m. Two-tailed unpaired Student's *t*-test. For box plots, the box spans from the 25th to 75th percentiles and the centre line was plotted at the median. Whiskers represent minimum to maximum range.

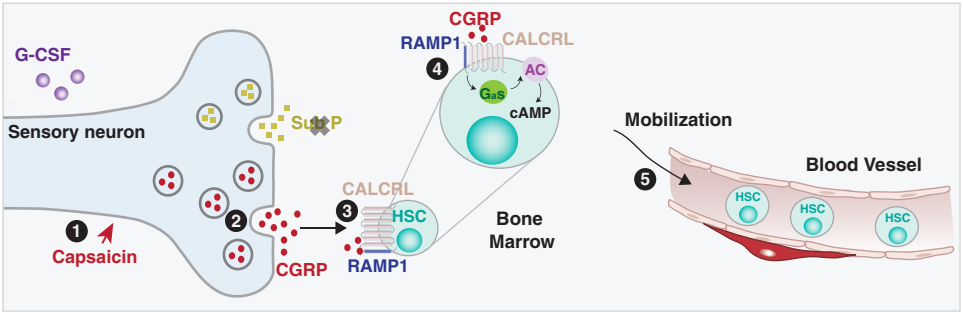

Extended Data Fig. 10 | Nociceptor-mediated HSC mobilization. Schematic representation showing that nociceptive-nerve-derived CGRP, but not substance P, acts via CGRP receptors on HSCs to enhance their mobilization via a cAMP-mediated signalling pathway.

nature research

Corresponding author(s): Paul Frenette

Last updated by author(s): 2020/09/29

Reporting Summary

Nature Research wishes to improve the reproducibility of the work that we publish. This form provides structure for consistency and transparency in reporting. For further information on Nature Research policies, see Authors & Referees and the Editorial Policy Checklist.

Statistics

For all statistical analyses, confirm that the following items are present in the figure legend, table legend, main text, or Methods section.

n/a	Confirmed
☐	☒ The exact sample size (*n*) for each experimental group/condition, given as a discrete number and unit of measurement
☐	☒ A statement on whether measurements were taken from distinct samples or whether the same sample was measured repeatedly
☐	☒ The statistical test(s) used AND whether they are one- or two-sided *Only common tests should be described solely by name; describe more complex techniques in the Methods section.*
☐	☒ A description of all covariates tested
☐	☒ A description of any assumptions or corrections, such as tests of normality and adjustment for multiple comparisons
☐	☒ A full description of the statistical parameters including central tendency (e.g. means) or other basic estimates (e.g. regression coefficient) AND variation (e.g. standard deviation) or associated estimates of uncertainty (e.g. confidence intervals)
☐	☒ For null hypothesis testing, the test statistic (e.g. *F*, *t*, *r*) with confidence intervals, effect sizes, degrees of freedom and *P* value noted *Give P values as exact values whenever suitable.*
☒	☐ For Bayesian analysis, information on the choice of priors and Markov chain Monte Carlo settings
☒	☐ For hierarchical and complex designs, identification of the appropriate level for tests and full reporting of outcomes
☐	☒ Estimates of effect sizes (e.g. Cohen's *d*, Pearson's *r*), indicating how they were calculated

Our web collection on statistics for biologists contains articles on many of the points above.

Software and code

Policy information about availability of computer code

Data collection	Data collection was performed using FACS Diva 6.1 software (BD Biosciences) for FACS, Slide Book software 6.0 (Intelligent Imaging Innovations) for confocal microscopy imaging, and QuantStudio 6 Real-Time PCR Software (Applied Biosystem, Thermo Fisher) for quantitative real time PCR.
Data analysis	Data analysis was performed using either GraphPad Prism 8 (GraphPad Software, San Diego, CA), FACS Diva 6.1 software (BD Biosciences), FlowJo 10.4.0 (LLC), Slide Book software 6.0 (Intelligent Imaging Innovations), and QuantStudio 6 Real-Time PCR Software (Applied Biosystem, Thermo Fisher). RNA sequencing data were analyzed using Spliced Transcripts Alignment to a Reference (STAR) v2.6.1, HTSeq v0.6.1 and DESeq2.

For manuscripts utilizing custom algorithms or software that are central to the research but not yet described in published literature, software must be made available to editors/reviewers. We strongly encourage code deposition in a community repository (e.g. GitHub). See the Nature Research guidelines for submitting code & software for further information.

Data

Policy information about availability of data

All manuscripts must include a data availability statement. This statement should provide the following information, where applicable:

- Accession codes, unique identifiers, or web links for publicly available datasets
- A list of figures that have associated raw data
- A description of any restrictions on data availability

RNA sequencing data have been deposited in the Gene Expression Omnibus under accession number GSE156449 (https://www.ncbi.nlm.nih.gov/geo/query/acc.cgi?acc=GSE156449). Source data behind Figures 1-4 and Extended Data Figures 1-10 are available within the manuscript files.

Field-specific reporting

Please select the one below that is the best fit for your research. If you are not sure, read the appropriate sections before making your selection.

☒ Life sciences ☐ Behavioural & social sciences ☐ Ecological, evolutionary & environmental sciences

For a reference copy of the document with all sections, see nature.com/documents/nr-reporting-summary-flat.pdf

Life sciences study design

All studies must disclose on these points even when the disclosure is negative.

Sample size	No statistical method was used to predetermine sample size. Sample size was chosen based on previous studies performed in our lab.
Data exclusions	No data was excluded from the analysis.
Replication	Experimental replication was attempted at least three times for all datasets/figures shown, and experimental findings were reliably reproduced.
Randomization	Mice were randomly assigned to experimental groups including male and female mice.
Blinding	Investigators were not blinded to mouse genotypes during experiments. Data reported for mouse experiments are not subjective but rather based on quantitative flow cytometry. Data blinding was not possible for some experiments due to obvious difference in expansion or reudction of haematopoietic stem cells.

Reporting for specific materials, systems and methods

We require information from authors about some types of materials, experimental systems and methods used in many studies. Here, indicate whether each material, system or method listed is relevant to your study. If you are not sure if a list item applies to your research, read the appropriate section before selecting a response.

Materials & experimental systems

n/a	Involved in the study
☐	☒ Antibodies
☒	☐ Eukaryotic cell lines
☒	☐ Palaeontology
☐	☒ Animals and other organisms
☒	☐ Human research participants
☒	☐ Clinical data

Methods

n/a	Involved in the study
☒	☐ ChIP-seq
☐	☒ Flow cytometry
☒	☐ MRI-based neuroimaging

Antibodies

Antibodies used	The following antibodies were used for FACS: the anti-lineage panel cocktail (CD3e, B220, CD11b, Ter119 and Gr-1, at 1:100 dilution) was from BD Bioscience (559971), anti-Sca-1-FITC (D7; 11-5981-85), anti-CD117(c-Kit)-PE/Cy7 (2B8; 105814), anti-CD48-PerCP-eFluor710 (HM48-1; 46-0481-85), anti-CD150-PE (TC15-12F12.2; 115904), anti-B220-APC-eFluor780 (RA3-6B2; 47-0452-82), anti-CD3e-PerCP-Cy5.5 (145-2C11; 45-0031-82), anti-Gr-1-FITC (RB6-8C5; 11-5931-85), anti-CD11b-PE (M1/17; 12-0112-83), anti-CD45.1-PE/Cy (A20; 25-0453-82), anti-CD45.2-FITC (104; 109806), anti-Sca-1-APC (D7; 17-5981-83), anti-CD117-BV421 (2B8; 105828), anti-CD45-PerCP-Cy5.5 (30-F11, 45-0451-82), anti-Ter119-PerCP-Cy5.5 (TER-119; 45-5921-82), anti-CD31-PE/Cy7 (390; 25-0311-82), anti-CD51-PE (RMV-7; 12-0512-83), anti-PDGFRα (CD140α)-APC (APA5; 17-1401-81), anti-Gr-1-APC (RB6-8C5; 17-5931-82), anti-F4/80-PE (BM8; 123110), anti-CD115-PE/C7 (AFS98; 25-1152-82), streptavidin APC-eFluor 780 (47-4317-82), anti-CXCR4-AF647 (L276F12, 146504), anti-CD49d-APC (R1-2, 17-0492-82), anti-CD44-APC (IM7, 17-0441-82), all purchased from BioLegend or eBioscience. Unless otherwise specified, all antibodies were used at a 1:100 dilution. Antibodies used for immunofluorescence imaging: anti-CD31-Alexa Fluor 647 (MEC13.3; 102516; BioLegend; 7.5 µg antibody/ mouse for injection), anti-CD144 (VEcadherin)-APC-Alexa Fluor 647 (BV13; 138006; BioLegend; 7.5 µg antibody/mouse for injection), anti-Tyrosine Hydroxylase (TH) antibody (Cat: AB152; Lot: 2493925; Millipore; used at 1:100), Alexa Fluor 488 conjugated anti-Tubulin Beta3 (Tubb3) antibody (Clone: AA10; Cat: 657404; Biolegend; used at 1:100), anti-CGRP antibody (Abcam ab36001; used at 1:1000). Secondary antibodies: donkey anti-rabbit IgG BV421 (406410, BioLegend), donkey anti-goat IgG AF568 (A11057, Invitrogen), donkey anti-rabbit IgG AF488 (A21206, Invitrogen), donkey anti-goat IgG AF488 (A11055, Invitrogen) and secondary antibodies were used at 1:200 dilution.
Validation	Antibodies were validated in previous studies performed in our laboratory (see references 3-6, 13, 28).

Animals and other organisms

Policy information about studies involving animals; ARRIVE guidelines recommended for reporting animal research

Laboratory animals	Nav1.8-Cre mice were a gift from Dr. John Wood (University College London). Nav1.8-Cre mice were bred with iDTA mice (both from Jackson Laboratory) and iTdTomato mice (from Jackson Laboratory) to generate Nav1.8-Cre/iDTA nociceptor-deficient mice for functional studies and Nav1.8-Cre/iTdTomato mice for imaging experiments, respectively. Ramp1–/– mice were generated in the 129S6/SvEv background29. All experiments with Ramp1+/+ and Ramp1–/– mice were carried out using littermates by intercrossing Ramp1+/- heterozygous mice. Carcrlf/f mice were generated as previously described30 and were bred with Vav1-iCre mice from Jackson Laboratory to conditionally delete Calcrl in haematopoietic cells. C57BL/6 CD45.1 and CD45.2 congenic mice were purchased from the Jackson Laboratory. Unless indicated otherwise, eight- to ten-week old mice of both genders were used for experiments. All mice were maintained in pathogen-free conditions under a 12h:12h light/dark cycle, temperature 68-72°F, humidity 40-70% and fed with autoclaved food.
Wild animals	No wild animals were used
Field-collected samples	No field-collected samples were used
Ethics oversight	This study complied with all ethical regulations involving experiments with mice, and all experimental procedures performed on mice were approved by the Animal Care and Use Committee of Albert Einstein College of Medicine.

Note that full information on the approval of the study protocol must also be provided in the manuscript.

Flow Cytometry

Plots

Confirm that:

☒ The axis labels state the marker and fluorochrome used (e.g. CD4-FITC).

☒ The axis scales are clearly visible. Include numbers along axes only for bottom left plot of group (a 'group' is an analysis of identical markers).

☒ All plots are contour plots with outliers or pseudocolor plots.

☒ A numerical value for number of cells or percentage (with statistics) is provided.

Methodology

Sample preparation	Peripheral blood was harvested by retro-orbital bleeding of mice anesthetized with isoflurane and collected in polypropylene tubes containing EDTA. Blood parameters were determined with the Advia120 Hematology System (Siemens). BM cells were obtained by flushing and dissociating using a 1-mL syringe with phosphate-buffered saline (PBS, Corning) via a 21-gauge needle. For analysis of stromal and endothelial cell populations, intact flushed BM plugs were digested at 37°C for 30min in 1 mg/mL collagenase type IV (Gibco), 2 mg/mL Dispase (Gibco) and 500 µg/mL DNase I (Sigma-Aldrich) in Hank's balanced salt solution (HBSS, Gibco). For FACS analysis and sorting, red blood cells were lysed and washed in ice-cold PEB (PBS containing 0.5% BSA and 2 mM EDTA) before staining with antibodies in PEB.
Instrument	BD LSRII Special Order System (BD Bioscience) was used for all data acquisition (H55100027). MoFlo Astrios EQ (Beckman coulter) was used for sorting experiments.
Software	Data was collected using BD FACSDiva 6.1 (BD Biosciences) software. Data was analyzed with FACS Diva 6.1 software (BD Biosciences) and FlowJo 10.4.0 (LLC).
Cell population abundance	Purity of cells sorted or analyzed was determined by their appropriate frequency and absolute numbers determined for control wild-type mice according to previous studies. It was described in the literature that HSCs comprise ~ 0.01% of total bone marrow. We have previously shown that MSCs are ~0.05% of total bone marrow. In every experiment, we included a control group. Because the sorted populations are very rare, we did not routinely carry out post-sort analysis.
Gating strategy	For all flow cytometric analysis and sorting debris were excluded by FSC, SSC scatters and DAPI (4', 6-diamino-2-phenylindole) staining was used to exclude dead cells, following which specific population were gated according to prior experience with doing similar experiments in our laboratory. Hematopoietic stem cells (HSCs) were identified as previously described in the literature: negative for lineage (CD3e, B220, Gr-1, CD11b, Ter119), negative for CD48 and positive for Ly6A/E(Sca-1), CD117 (c-Kit) and CD150 (SLAM markers), as depicted in Figure 4i (blood) and Extended Data Figure 2c (bone marrow). All other FACS analyses, donor derived CD45.2 cells in transplantation setting, myeloid cells (CD11b+), B cells (B220+), T cells (CD3e+) have all been described previously (see manuscript for citations describing similar studies done in our laboratory).

☒ Tick this box to confirm that a figure exemplifying the gating strategy is provided in the Supplementary Information.